EM STIMULATION OF WATER
FOR GEOTECHNICAL APPLICATIONS

by

Harlan Dwight Olson Sangrey

A thesis

submitted in partial fulfillment

of the requirements for the degree of

Master of Science in Civil Engineering

Boise State University

May 2011

BOISE STATE UNIVERSITY GRADUATE COLLEGE

DEFENSE COMMITTEE AND FINAL READING APPROVALS

of the thesis submitted by

Harlan Dwight Olson Sangrey

Thesis Title: EM Stimulation of Water for Geotechnical Applications

Date of Final Oral Examination: 04 April 2011

The following individuals read and discussed the thesis submitted by student Harlan Dwight Olson Sangrey, and they evaluated his presentation and response to questions during the final oral examination. They found that the student passed the final oral examination.

Arvin Farid, Ph.D.	Chair, Supervisory Committee
Jim Browning, Ph.D.	Member, Supervisory Committee
Elisa H. Barney Smith, Ph.D.	Member, Supervisory Committee
Sondra M. Miller, Ph.D., P.E.	Member, Supervisory Committee

The final reading approval of the thesis was granted by Arvin Farid, Ph.D., Chair of the Supervisory Committee. The thesis was approved for the Graduate College by John R. Pelton, Ph.D., Dean of the Graduate College.

ACKNOWLEDGEMENTS

I would first like to thank my advisor, Dr. Arvin Farid, for giving me the opportunity to participate in this project. I would like to also thank Dr. Jim Browning, my co-advisor and committee member for his constant support and advice. I would like to thank Dr. Elisa Barney Smith and Dr. Sondra Miller for generously participating in my committee. Thanks to Adam Spiegleman for his design and build of many pieces of equipment, especially the three-axis translation table. Thanks to Jon Rocha for his assistance and friendship in the lab. Most of all, thank you to my family who are always patient and supportive.

This research was supported by the National Science Foundation, under Grant No. IDR CBET-0928703, and the Department of Civil Engineering at Boise State University.

DEDICATION

This work is dedicated to my grandmother, Beverly Olson, for her timeless love and support.

ABSTRACT

The task of cleaning soil and/or groundwater contaminated by leakage from aging underground gasoline or petrochemical tanks along with surface spills of gasoline and other hazardous chemicals is of utmost importance for federal and state environmental agencies. Traditional clean up and contaminant removal involves dig-and-treat methods that are costly and impractical for large, contaminated sites. Less disruptive remediation techniques, such as air sparging, have become more attractive in the past decade. Air sparging, bioventing, and other remediation technologies that use air injection into soil can become very effective for non-aqueous phase liquid (NAPL) removal using volatilization and bioremediation. However, the effectiveness of methods such as air sparging is limited by the restriction of airflow. The majority of the injected air in air sparging flows through narrow air channels formed in the soil and water matrix, which forms a limited mass transfer zone (MTZ) for contaminant removal. Diffusion of air between these air channels, even though very slow, can help the cleanup. Pulsation of the air sparging pumps is among the only existing methods used to enhance airflow, but it is time-consuming and unable to create a controlled and uniform airflow pattern.

In this thesis, use of electromagnetic (EM) stimulation to expedite air sparging is investigated. A relatively high-power electromagnetic field is radiated into the water by utilizing a co-axial antenna connected to an EM source. The alternating electric field emitted into the medium can stimulate different mechanisms in the medium. As a result, the stimulated water molecules enhance diffusion of air and contaminant. This thesis

shows the first step in the study of EM stimulation on air and contaminant flow through saturated soils via an analogous demonstration of the effect of EM waves on diffusion of a non-reactive dye in water. It is successfully demonstrated in this work that the EM stimulation of the water and dye controls and changes the direction and rates of dye transport. The relation between the EM power input radiated into the medium and the change in the transport of the dye is also studied.

TABLE OF CONTENTS

LIST OF FIGURES

1. INTRODUCTION

1.1 Motivation

Environmentally hazardous spills of chemicals/petrochemicals and gasoline are a serious concern when contaminating ground water. There is an increasing need for cleanup of these types of spills -- a need not expected to diminish in the foreseeable future, as large numbers of underground chemical/petrochemical and gasoline storage tanks around the country and world are aging and beginning to leak or have been leaking for years. The contamination due to these spills can seep into the ground, and without any treatment, the problem can spread to drinking water. If left untreated, the spill will take tens or hundreds of years to dilute and degrade to a level accepted by drinking water standards. The ability to treat large areas of spillage in an efficient and cost-effective manner is necessary for feasibly faster treatment of contaminated sites. Removal of contaminated soils can be very intrusive and expensive. Hence, other methods of spill clean-up are more attractive.

Many methods of spill remediation are in use today, and the efficiency and effectiveness of these methods are being improved constantly. Air sparging is an increasingly popular method for remediation of sites contaminated with non-aqueous phase liquid (NAPL) spills. The method of pumping air into the contaminated groundwater is shown to be effective in reducing contamination via volatilization to acceptable levels. However, the air sparging process can take months or years and can,

therefore, be very costly. Air sparging is limited by random air channel formation (Elder and Benson, 1999), which creates a limited mass transfer zone (MTZ) between the medium and formed air channel (Braida and Ong, 2001). One of the main existing methods to enhance air sparging's effectiveness is pulsating, which is both time-consuming and uncontrolled. Vermeulen and McGee (2000) have examined electromagnetic (EM) bioheating and have shown this process to be successful for enhancing the removal of volatile organic compounds (VOCs). However, only preliminary work was performed, and the process was not controlled. The EM heating process also enhanced the removal via increasing the soil temperature to 100^{o}C, which harms bacteria that digests contaminants also present in soil.

The current research, developed in this thesis, focuses on the major goal of using electromagnetic (EM) stimulation to expedite air sparging without any considerable or even measureable temperature change. The first step is to determine the effects of EM stimulation on diffusion. The diffusion of a non-reactive dye in water was used as a visible analogy to air sparging in saturated soil. This work is based on the hypothesis that stimulation of the media will expedite diffusion of the non-reactive dye in water and that a relationship between diffusion rate to different frequencies and power levels of EM stimulation can be correlated.

1.2 Scope

To test the hypothesis, stated above, this research investigates the effects of EM stimulation on diffusion. Studies were performed to quantify the effects of the EM stimulation on the diffusion of an inert and non-reactive dye in water. Stimulated and

non-stimulated tests were performed for comparison, and the EM field was mapped for accurate field analysis and correlation to diffusion rates. It is noteworthy that diffusion is the mechanism expected for the transfer of air. However, the research will demonstrate that the stimulated case is governed by a more complicated regime. Transfer analysis was performed using digital images to determine temporal and spatial concentration changes.

2. BACKGROUND

2.1 Remediation Techniques

There are many techniques to cleanup environmental spills. Gasoline and other volatile chemicals that leak from a tank or seeped from surface spills into the soil have proven very difficult to remove from soil. The ex-situ method of excavation and removal of contaminated soils is very expensive and destructive, and hence, ineffective for large spills, especially when the contaminants are mobile. Nevertheless, this technique has been used for many years. Alternatives to excavation and treatment have been developed with different levels of effectiveness.

Bioventing is a method used in unsaturated soils for remediation (Dupont 1993). Bioventing utilizes low-volume airflow in soil to promote microbial activity and biodegradation. The transfer of oxygen to in-situ organisms enables aerobic metabolization of contaminants. Bioventing injection is often used in conjunction with an extraction well to help remove the vapors from the soil but is insufficient on its own to clean up a large spill.

Slurping is another method used to remove contaminants, usually oil or light non-aqueous phase liquids (LNAPLs), from the top of the groundwater table. In slurping a vacuum is used to "slurp" the layer of less dense and water-phobic oil or LNAPLs that is in the region above the water table and beneath the vadose zone (Weingardt and Gonzales, 2002). Normally, large amounts of water and vapors are removed and treated

as part of this remediation process. The hydrocarbon contaminants are removed before the water is returned to the ground.

Steam injection is another method of in-situ remediation. In this method steam is pumped into the ground to help the volatile compounds to vaporize. The vapor can then be removed more easily with an extraction well (Falta, 2001). Although less effective, vacuum extraction-wells are used as stand-alone tools for remediation.

Although there are many commercially available methods for spill remediation, the efficiency and effectiveness of these methods differ. Air sparging is a very attractive remediation technique currently employed throughout the world because air sparging offers a less invasive, yet effective, remediation process. Pumping air into the groundwater to remove volatile contaminants in conjunction with soil vapor extraction wells has proven effective in treating spills. Air sparging does, however, have limitations, particularly the speed and effectiveness of the remediation.

One of these limitations is the formation of air channels and the slow diffusion to remove the contaminants. Braida and Ong (2001) pointed out that the limiting factor of air sparging was the size of the mass transfer zone (MTZ). The MTZ is the area surrounding individual air channels through which air diffuses and treatment of contaminants occurs. They found that the MTZ ranged from $71D_{50}$ to $215D_{50}$ (D_{50} = mean particle size) for low organic carbon content media. An illustration of the MTZ is shown in Figure 2.1.

The limiting effect of the size of the MTZ surrounding each air channel on the treatment process encourages many researchers to find new methods of expanding this effective zone. Semer et al. (1998) call the area around the air sparging well, including all

channels and their corresponding MTZ, the radius of influence (ROI).

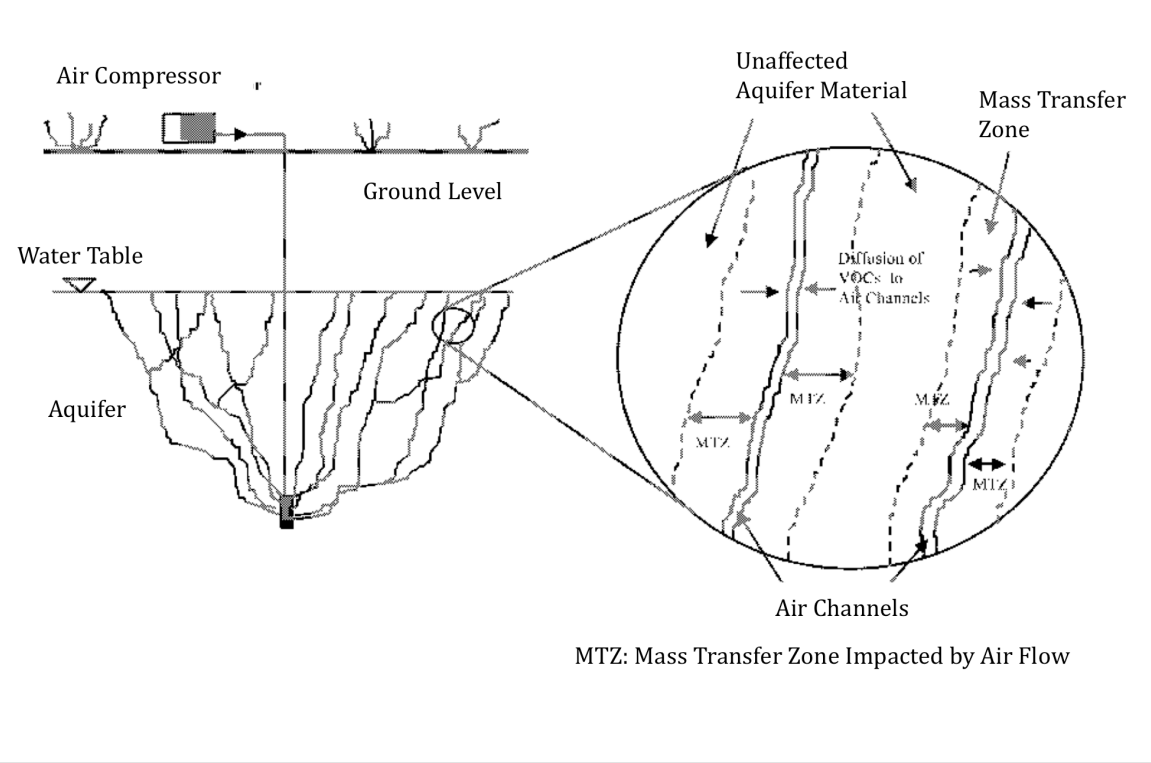

Figure 2.1: Mass Transfer Zone (Braida and Ong, 2001)

2.2 Air Sparging

This review will discuss past works pertaining to air sparging and the limitations thereof. As demonstrated in the following, studies performed by several researchers showed that air channel formation is a major limiting factor for air sparging systems. Air sparging is limited by the mass transfer zone (MTZ) and radius of influence (ROI), which were investigated by Braida and Ong (2001) and Semer et al. (1998), respectively. Elder and Benson (1999) studied related limitations of air sparging by looking at air channel formation during air sparging. Tsai's (2007) studies of air sparging bridged the other studies and looked at the air channels and their formation around the in-situ air sparging wells. Some efforts have been made to expedite VOC remediation, such as the EM

heating (Vermeulen and McGee, 2000), but have been limited to only the vadose zone. The most relevant work done by Braida and Ong (2001) will be discussed last.

Semer et al. (1998) give a general description of air sparging techniques involving multiple injection wells paired with vacuum wells leading to a vapor treatment unit. To distinguish between LNAPLs and DNAPLs, the author's looked at the life expectancy of the contamination. Defining an appropriate radius of influence (ROI) is important in ensuring all contaminated regions are treated. Typical ROIs are shown in Figure 2.2.

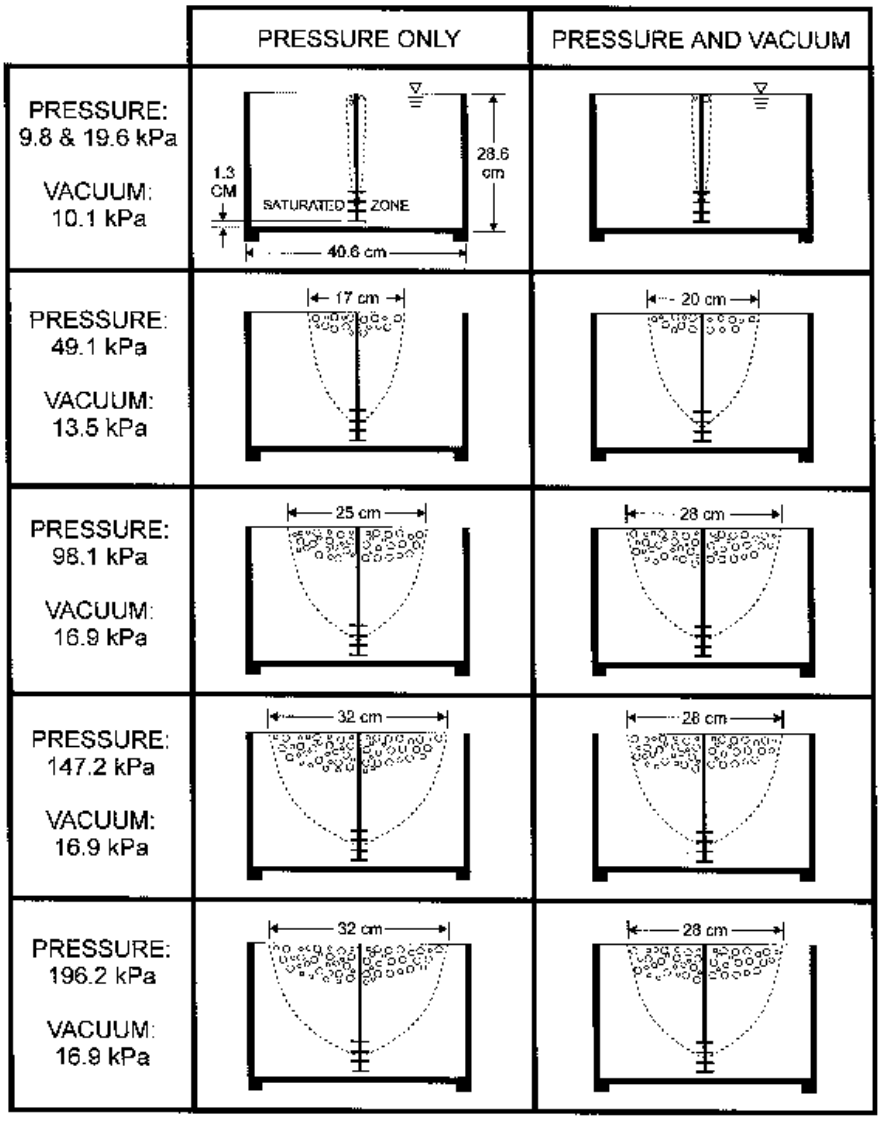

Figure 2.2: Radius of Influence (Semer et al., 1998)

With some analysis of the site, a good prediction of the ROI can be established. Subsurface conditions can impact the effectiveness of the air sparging. For example, air channels are formed but can be blocked by lenses of low permeability soils (e.g., clay lenses); in granular soils and at low flow rates, bubbles are formed instead of channels. It is observed that there is a limited area of influence when pressure is increased; however further increases in pressure result in an increase in the vigor of bubbles and not an increase in the area. Observations from the top of the soil, during sparging at different depths and pressures, revealed channeling. Semer et al. (1998) demonstrated that deeper soil/injection depths result in channeling further from the sparging well. The deeper injection allows for more time for the channels to migrate more horizontally as the air travels vertically. Even in deep soils, a limit to the ROI is observed. In sand a greater entry pressure is needed to overcome the hydrostatic and capillary pressures, and thus the ROI is much larger for sandy soils than fine gravel. For gravel, there is no channeling and the air rises randomly to the surface in free bubbles. Larger pressures are required in sand to overcome and create channels. Once channels are formed, the pressure may be lowered to a point and still maintain adequate flow.

Studying the limiting factors of these channels, Elder and Benson (1999) performed a bench top study of the air channels that formed. It is known that air sparging forms air channels in-situ and that these channels can be macroscopic and commonly form in coarse media, such as gravels, or much smaller particle sizes. The smaller air channels, called “pore-scale,” occurred in the medium with smaller diameter particles. These channels usually form a cone or parabolic shape as they rise to the surface and away from the source, as shown in Figure 2.2 by Semer et al. (1998). To measure and

model the gasses and the amount of VOCs transferred, assumptions of the average outer area of a single bubble are made using estimates from similar situations in formations through unsaturated porous soil. The size and tortuosity of the channels are used to calculate an approximate value of the interfacial area between the sparging gas and the contaminated liquid. Calculating the theoretical mass transfer with these conditions, a total effect could be modeled. A similar setup to the one used by Rutherford and Johnson (1996) will be used in future research to observe the airflow rates in and out of a controlled sparging tank. The gasses are pumped into a medium of glass beads and collected at the top measuring the airflow rates. Their setup is shown in Figure 2.3.

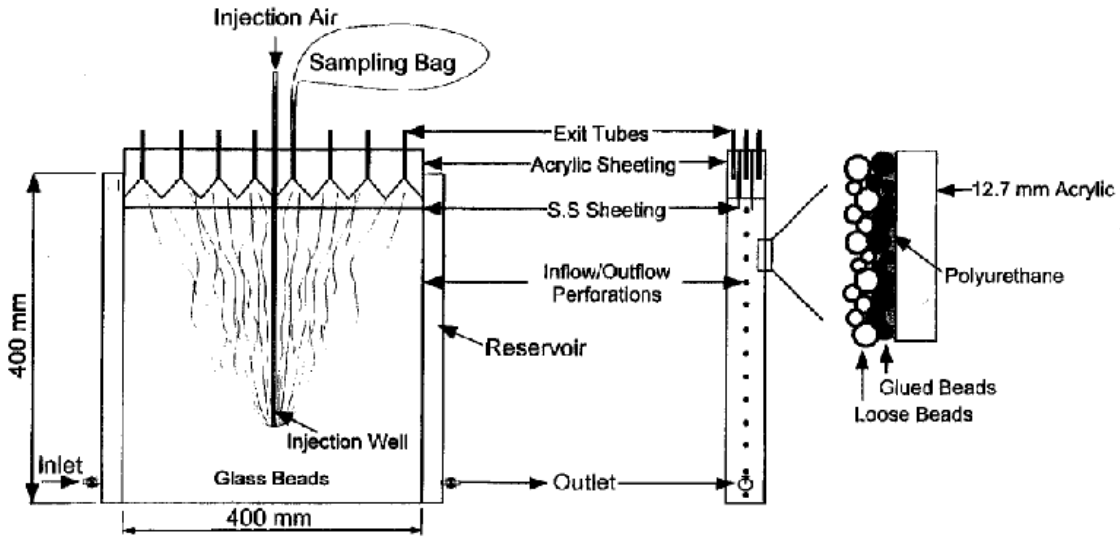

Figure 2.3 : Experimental Setup used by Elder and Benson (1996)

Elder and Benson's tests were performed at different pressures and flow rates in three media with different glass-bead sizes (small, larger, and mixed). With coarse beads, backlighting was used, and with fine beads, front lighting was used. The air channels showed up as dark lines because they did not transmit light. The formed channels were V-shaped at lower pressure and U-shaped at higher pressures. The channels, in all cases,

were pore-scale channels (Clayton, 1998). The diameters of the channels were fairly uniform and varied (< 27%) only at intersections and at splits in the channel.

Particle mobilizations effect on flow-paths had not been considered before Tsai (2007). Tsai studied the smaller particles, which were moved with the water displacement induced by air channels during air sparging. The tests were conducted on a much larger scale in a mostly homogeneous silty sand site. The air sparging well was drilled with monitoring well sites surrounding to a radius of >10 m. The well was run with a tracer gas to observe the airflow influence and tracked by the surrounding monitor wells. The data indicated that the preferential paths for the airflow were within 2.6 m from the sparging well. This is relative to the 7.48-m sparging depth. The study concluded that the majority of the airflow was concentrated around the sparging well. The channels were also subject to changes in porosity and permeability due to the movement of particles, as a result of the air sparging. These changes also affected the paths and locations of the channels.

All of these studies show that remediation of contaminants can take large amounts of time. Not many researchers have worked on enhancing air sparging. Some studies were conducted using EM heating to expedite remediation. Vermeulen and McGee (2000) and Price et al. (1999) studied the use of EM power to heat the soil and underground hydrocarbons. Vermeulen and McGee (2000) studied low (60 Hz) EM heating for changing the viscosity of energy fuels to promote removal and the use of EM heating in environmental industries. They demonstrated the use of EM power to heat the soil to bring the vapor pressures to a point where soil vapor extraction (SVE) was more useful. Price et al. (1999) performed a similar study focused solely on the uses for

remediation. Price et al. (1999) were able to document a temperature of 100^{o}C near the applicator and up to 40^{o}C, 1.5-m away. Price et al. (1999) also performed in-situ tests with a 25-kW radio frequency (RF) generator used in conjunction with air sparging and SVE wells. The results of the in-situ tests showed an increased removal of gasoline range organics (GRO). The use of in-situ heating was discussed without looking at the negative environmental impacts due to overheating of organisms. There is also no study of the impact of the RF stimulation other than heating.

Braida and Ong (2001) defined the mass transfer zone (MTZ) of the air sparging system as the area around the air channels impacted by the airflow. If the size of the MTZ is much smaller that the distance between air-channels, the air sparging time will significantly increase. The size of the MTZ is dependent on the soil and the VOCs to be removed. Transport of VOCs to the air-water interface and diffusion of air into the saturated medium are limiting factors. Their data strongly suggests that the volatilization of VOCs during air sparging may be controlled by the aqueous diffusion of VOCs through the porous media to the air channels. If diffusion and air channel size are the controlling factors of the MTZ, then an increase in either will provide more rapid remediation.

2.3 Theory

2.3.1 Stimulation and Technical Approach

The choice of frequency used for stimulation and the size of the apparatus for in-situ simulation are based upon different relaxation mechanisms (e.g., the Maxwell Wagner relaxation) of water at various frequencies as well as the dielectric properties of

the water. As shown in Figure 2.4, there are multiple relaxation mechanisms. Performing the experiment at frequencies below 1 MHz may not be practical due to the large wavelengths at these frequencies. Large wavelengths are not desired for the lab-scale experiment because too large of an apparatus would be required to create an entire wavelength in the medium. Hence, we focused on frequencies between 10 MHz to 1 GHz in the lab. Further frequency limitations are determined by the matching network, which will be discussed later in Section 3.3. Feasibility evaluation is performed at around 100MHz for a variety of reasons including availability of devices and the limitations of their effective frequencies.

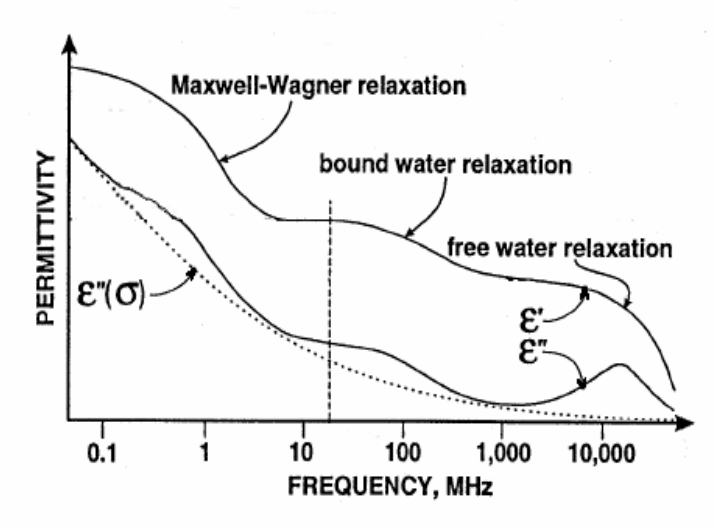

Figure 2.4: Dielectric spectrum of soil (Hilhorst, 1998)

Transmitting multiple wavelengths into the medium is ideal. However, this is not possible with the equipment available in the laboratory. The reason is that impedance matching between the medium and the amplifier using a matching network to prevent excessive reflection back into the amplifier is only possible at individual frequencies. The wavelength of an electromagnetic wave at 100 MHz in free-space is approximately 3 m. The wavelength of any wave is determined by medium and the frequency; in this case air

is the medium. The speed of light in air is approximately 3×10^8 m/s. The frequency (f) is in cycles per second and one cycle is one wavelength long. Therefore, the wavelength (λ) of light in air is defined as follows.

$$\lambda(m) = \frac{3.0 \times 10^8 (\frac{m}{s})}{f(Hz)} \tag{2.1}$$

The wavelength of the EM wave inversely varies with the square root of the relative dielectric permittivity or constant (ε_r) which is the ratio between the dielectric permittivity of the medium to that of vacuum. The relative dielectric permittivity of water can be as high as 81. Hence, the wavelength in water for a frequency of 100MHz is approximately 0.333 m. This relationship will be discussed further in the results section of this work. Based upon this analysis, the apparatus will be approximately 1/3 m in length, and the frequency range will be approximately 100 MHz.

Dielectric permittivity (ε) describes the polarization and susceptibility of a material to the application of an electric field. Dielectric permittivity can be complex and can be divided into real and imaginary parts:

$$\varepsilon_r(\omega) = \varepsilon_r'(\omega) + j\varepsilon_r''(\omega) \tag{2.2}$$

where ε_r is the permittivity ratio; ω is the angular frequency ($\omega = 2\pi f$ where f is the linear frequency), ε'_r is the real component and ε''_r is the imaginary component. The frequencies chosen for this experiment are related as much to the equipment and matching network as to the physical constraints of the medium.

2.3.2 Dielectrophoresis, a Potential Mechanism behind EM Stimulation

Dielectrophoresis is the phenomenon where non-charged particles can experience a force in a medium created by an electric field gradient. By inducing a polarization, the particles exhibit the ability to have a net force due to an electric field gradient regardless of their charge. The result of this force is dependent on the electric properties of both the medium and the particle, as well as the size of the particle and the frequency of the electric field. Although dielectrophoresis is most readily observed for particles with diameters ranging from 1-1000 μm, the 1-5 nm dye used in this experiment can still be affected. The force that can be exerted from the dielectrophoresis is dependent on the complex dielectric constant of the particle (ε_p^*) and of the surrounding medium (ε_m^*). This relationship is described in Equation 2.3.

$$F_{DEP} = 2\pi r^3 \varepsilon_m \mathrm{Re}\left\{\frac{\varepsilon_p^* - \varepsilon_m^*}{\varepsilon_m^*}\right\}\nabla\left|\vec{E}\right|^2 \tag{2.3}$$

where $\vec{E}$ is the non-uniform electric field and r is the radius of a homogeneous sphere with no net charge (the particle). This force is proportional to the gradient of the magnitude of the electric field squared.

When the dielectric permittivity of the particle is higher than that of the medium, the particle will move toward the area of lower electric field intensity. In a case where the dielectric permittivity of the medium is higher than that of the particle, the particle will move, against the gradient, toward the area of higher electric field intensity. The effects of dielectrophoresis are frequency-dependent for each medium and particle combination.

The results of this work will look to clarify and confirm whether dielectrophoresis is the controlling mechanism in the tests or not.

2.3.3 Diffusion Theory

The mathematical tools that model diffusion employ a partial differential equation (PDE) to incorporate the variables influencing the physical mechanism of matter transport. The theory that every particle moves in a random direction depending on its interactions with the surrounding random particles is at the root of these models. The mathematical tools represent the diffusion that is observed in an ideal physical world. The theory that describes this movement is called the random walk of particles. The theory holds that any given particle can and will travel in random directions when interacting with other similar particles acting in the same way. A given particle will travel through the area defined by its boundaries and can travel across the entire area or just a small corner with no more likelihood of either pattern. Furthermore, if the medium is homogeneous, there will be no net changes in concentration within a defined system.

Although the movement of individuals is random, if there is a gradient in the concentration of the quantity there will be a net flux in the system. This gradient will be reduced until the net flux of the system leads to the gradient approaching zero.

Some of the fundamental mathematical representations of the diffusion process that are currently accepted are shown in the following. Without solving any of these equations, the effect created through the approach outlined later in this text will be shown.

Fick (1855) was the first to quantify the molecular diffusion process by applying the conduction of heat equations developed by Fourier (1822). This theory states that the rate of diffusion is proportional to the gradient of concentration of the substances.

$$F = -D\frac{\partial C}{\partial x} \tag{2.4}$$

where F is the transfer rate, C is the concentration of the diffusing material, x is the movement direction in this 1D (one-dimensional) flow, and D is the diffusion coefficient. This relationship is called Fick's first law. His second law relates the diffusing material concentration and the diffusion coefficient over space and time. The change in concentration over the change in time is a rate of change related to the concentration flux and the diffusion coefficient. Hence, for a homogeneous and isotropic medium

$$\frac{\partial C}{\partial t} = D\frac{\partial^2 C}{\partial x^2} \tag{2.5}$$

For a 3D (three-dimensional) diffusion, again assuming the medium is homogeneous. This equation can be expanded to all directions. This is the simple case where x, y, and z are the primary axis and D is not spatially dependent, but not equal in all axes. If the diffusion coefficient, D, is time dependent, then a time-dependent D ($D = f(t)$), and $dT = f(t)dt$ can be used. For a generally anisotropic but homogeneous medium

$$\frac{\partial C}{\partial t} = D_x\frac{\partial^2 C}{\partial x^2} + D_y\frac{\partial^2 C}{\partial y^2} + D_z\frac{\partial^2 C}{\partial z^2} \tag{2.6}$$

with the same spatially dependent variables as above. The diffusion equation can be solved in each case, which leads to a spatial and temporal solution. The result of diffusion over a near infinite time is that the concentration gradient will go to zero, and therefore, the net flux of the system will go to zero as well. These cases are all idealized assuming a

constant diffusion coefficient. The diffusion equation must take into account any external forces and their effect. One of the uncontrolled external forces in any diffusion tests on the Earth's surface is gravity. It will later be shown that EM stimulation is also an external force that can dominate diffusion.

In any system, there will be external contributing factors. The Earth's surface is often thought of as an inertial reference frame, but the influence of gravity should not be ignored. In diffusion, gravity can play a part as an external (in a way diffusing) force acting on the system. This force will influence particles of greater density relative to the others. In many media gravity can create a gradient in concentration.

3.0 MATERIALS AND METHODS

To experimentally model the stimulation of groundwater, a series of bench-top tests were conducted with several apparatuses. The objective, covered in this thesis, is to demonstrate that EM waves stimulate the medium through a mechanism beyond heating. In other words, the main motivation behind selection of EM stimulation is to demonstrate that the frequency of EM waves can be controlled to reduce the generated heat to maintain the temperature of the medium while simultaneously showing signs of stimulation. Hence, the stimulating effect of temperature increase (thermal heating) is compared with EM stimulation with monitored temperature.

The first series of tests used an inert non-reactive dye to compare the effect of temperature and EM stimulation on diffusion. The tests, in which thermal heating is used, are herein called thermal tests. The comparison between the thermal and EM stimulation effects are studied using two different approaches by: (i) comparing the thermal temperature increase that can create the same level of diffusion stimulation as EM waves and (ii) comparing the level of diffusion of the EM stimulated tests with the non-stimulated tests at the same medium temperature. The second series of tests consisting of EM-stimulated tests use a submerged CPVC-encased monopole antenna as the source of EM stimulation. The monopole antenna is an N-type coaxial cable with 70 mm of the conducting shield stripped, placed in a CPVC casing, and submerged in the medium. The series of diffusion tests that use the submerged CPVC-cased monopole antenna were performed in a 40 cm × 40 cm × 40 cm clear acrylic cube while the thermal tests were

performed in a 1000-mL volumetric flask. The volumetric flask and acrylic cube were used to enable visualization of the diffusion.

The water used in the EM tests was de-ionized and de-aerated before each test. Using the de-aerated water is very important to prevent generation of air bubbles in order to acquire clean images for analysis. When non de-aerated water was used, gaseous air bubbles formed on the surfaces of the acrylic box, creating obstructions and error in the image analysis. De-ionized water was provided through a laboratory supply, which was accessed from a tap at the sink in a lab. Deaeration was performed using an ELE brand Water De-Airing System that was run to deaerate the water for at least 45 min per batch. The test medium was approximately 13 L, so several batches were required to fill the 56 L apparatus. Once the apparatus had been filled, it was left overnight to settle any turbulence and come to a uniform temperature.

3.1 Thermal Tests

The thermal tests were performed in the laboratory using a water-bath, to keep the test volumetric flask at a constant temperature. During preliminary tests and because the dye is more dense than water, it was observed that the dye rapidly descended through a splash-like turbulence propagation. Therefore, the dye for the thermal tests was injected at the bottom of the medium to minimize any advective mixing mechanism, which would compromise observations of the diffusion. The temperature of the test medium and water-bath were monitored closely to ensure no rapid thermal changes. Glass (non-metallic) thermometers were used in the test medium and water-bath for this purpose. The water used as the test media was from the tap, and the dye used was McCormick® green food

color. The dye was introduced into the water in the volumetric flask and the time was recorded. The total elapsed time was recorded when the dye in the volumetric flask reached steady-state (uniform concentration).

3.2 Dye Injection for EM Stimulation

Using a pipette, the dye for EM stimulated tests was delivered to the center of the acrylic injection table in the water tank. The dye was injected into a concave depression ground on top of the acrylic table. This table allows the dye to be introduced to the middle of the test medium without immediately flowing away. A CPCV pipe passes through the middle of the injection table and concave depression, which encapsulates the antenna for some of the tests. The pipette, for injecting dye, was taped to this CPVC pipe to avoid any agitation in the water. Before filling the box with water, a rubber septum was placed on the opening of the pipette, sealing the top and not allowing the pipette to fill with water. For dye injection, a syringe was used to inject a carefully measured amount of dye (1.2 g) into the pipette, which exited onto the concave portion of the injection table. The septum and syringe are shown in Figure 3.1.

The dye was first measured in a vial on the scale to ensure a consistent proportion was maintained. This vial was capped with a penetrable cap for removal of the dye with the syringe. This method ensures consistent measurements and dye injections.

Figure 3.1: Dye injection septum and syringe

3.3 EM Stimulated Diffusion Tests

The experiments of this task were performed in a 40 cm × 40 cm × 40 cm clear acrylic cube stimulated with a relatively high-power (50W) RF signal into our system creating the EM waves. The equipment for creating this stimulation is discussed in Section 3.5.

The medium and dye in the test apparatus were stimulated by a monopole antenna, cased in a CPVC pipe, and submerged in the medium. The entire system was placed in a large Faraday cage to contain the EM waves, to prevent interference from

outside the experiment, and to protect researchers, as high-power EM waves can be harmful, if not contained (Jamieson et al., 2007). A wooden frame with an aluminum screen stretched across was assembled and carefully grounded with a removable door for access to create a uniformly conducting cage, although the door was not used during testing. All seams for the box were taped using aluminum tape to ensure conduction. The test apparatuses for the thermal and first EM-Stimulation tests are shown in Figure 3.2.

The diffusion tests are the main experiments for this portion of the investigation. To study the effects of the EM stimulation on diffusion, a controlled and reproducible environment to compare diffusion rates was created. There are several factors that can affect diffusion to maintain consistency and repeatability. The acrylic cube containing the testing medium was assembled from carefully cut rectangular pieces and cemented together with "WELD ON 4" acrylic cement. The construction created a watertight and rigid environment for testing allowing visual analysis of the diffusion.

A 40-cm sided cube was chosen to give the antenna, originally in the vertical position, a uniform and symmetric medium to stimulate. The antenna was submerged in water, which due to the lossy nature of water prevents the EM power from taking a preferential path between the antennas and surrounding boundaries. The relative dielectric permittivity of water is approximately 80 at 20^{o}C while that of air is approximately 1. This difference in permittivity means that the resistance of waves passing through water is 80 times greater than in air.

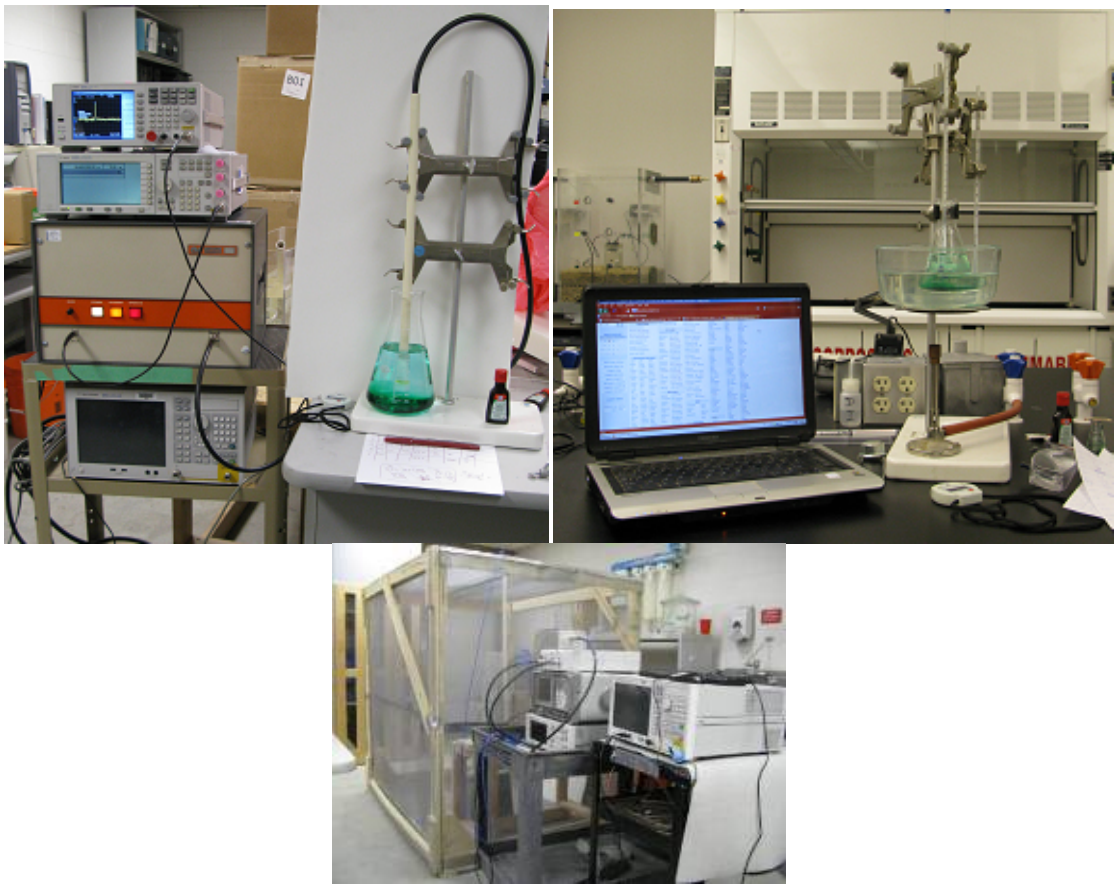

Figure 3.2: Setup and devices used for thermal (upper right) and EM stimulation (upper left and bottom) tests

The antenna used is an RG8 coaxial cable, discussed later, encased in a CPVC pipe. The exposed antenna was positioned in the center of the testing medium. The antenna and CPVC casing are bent in an L-shape to avoid drilling any opening in the vertical walls of the acrylic box.

The acrylic box used for the diffusion tests is made from 1-cm thick acrylic plates and a 1.2-cm thick bottom plate. The sides when assembled measure 40-mm outside edge to outside edge. The bottom measures 45-cm square and the walls are centered leaving an even gap all around. To stiffen the walls and prevent sag or failure, 2.5-cm wide stiffeners were added perpendicular to the walls creating a ridge 2-cm from the top edge.

All acrylic parts are joined using “WELD ON 4”, creating a watertight and optically clear joint. This assembly provides a stable environment to conduct our diffusion measurements while allowing for an unobstructed view for analysis. A clear acrylic table, referred to as the injection table, was built in a similar fashion. The injection table has a total height of 15-cm including the 1-cm top and bottom plates. The top is 10 cm × 10 cm while the bottom is 13 cm × 15cm, providing a stable base. The table was held in place by acrylic blocks glued to the bottom of the tank with silicone glue. The acrylic blocks glued with silicone to the bottom of the box restrict movement of the table while injection is taking place to ensure consistent images. The CPVC pipes, table, and acrylic box are shown in Figure 3.3.

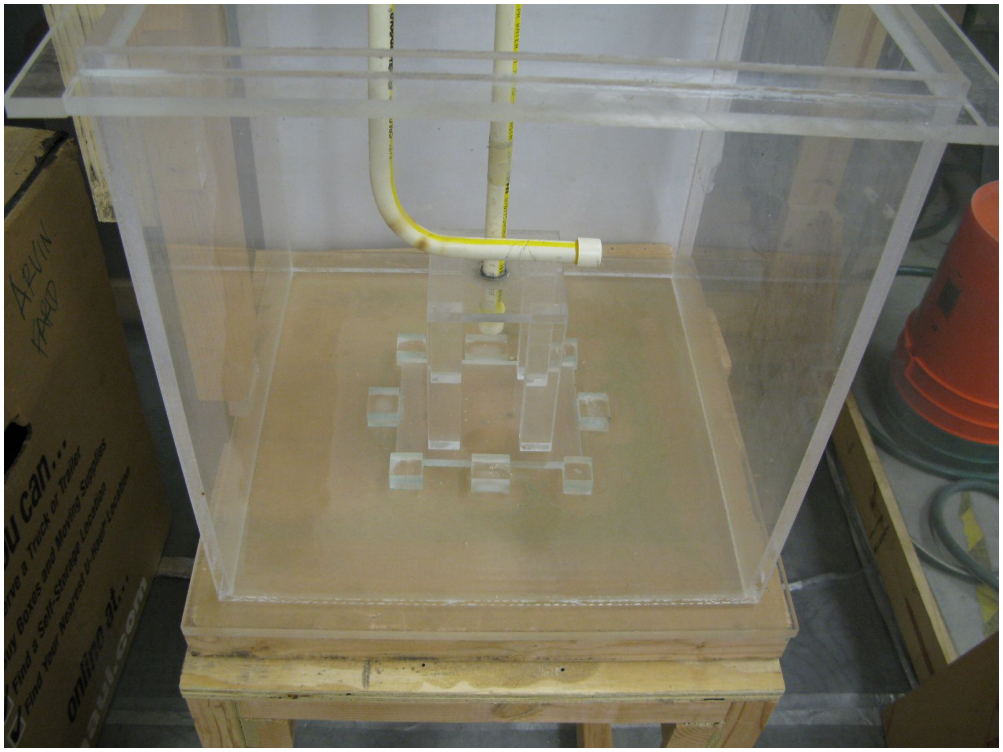

Figure 3.3: Acrylic Test Box, Dye Table, and CPVC Antenna Case

A CW (continuous wave) RF signal was generated using an HP E4400B signal generator. A Model 100LMB amplifier manufactured by Amplifier Research was used to

amplify the generated signal. To maximize the power output and reduce reflection back into the amplifier, the impedance of the source (Z_{source}) and the one of the load, in this case the medium (Z_{load}), must be equal,

$$Z_{source} = Z_{load} \tag{3.1}$$

A matching network is used to match the impedance of the medium to the one of the amplifier (50 Ω), which is the source impedance. The matching network is an L-shaped matching network shown in Figure 3.4. The L-shaped matching network circuit was built in a "BUD" box (i.e., aluminum box to contain the EM waves). This network is used to minimize the reflection at the interface between the medium of interest, the antenna, and the amplifier. Matching of the network ensures maximum power transfer into the medium and protects the amplifier. The matching network includes two 14-380pF variable two-gang capacitors, one in parallel, and one in series to tune the impedance of the testing medium to the impedance of the amplifier (50 Ω). The components are connected with 50Ω RG8 coaxial cables. This impedance matching is performed for a single frequency within the frequency range of optimum performance of the amplifier (50 MHz to 230 MHz).

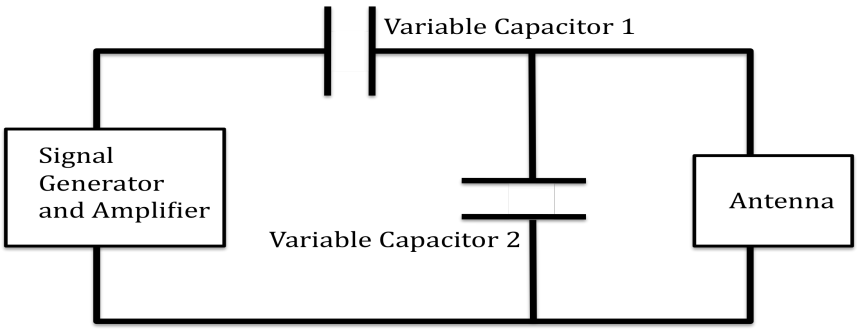

Figure 3.4: Schematic of network

To measure the circuit impedance for network matching, the system (i.e., the antenna submerged in the medium, the cables, and the matching network) is connected to

an Agilent Technologies E5071C vector network analyzer (VNA). Using a matching network by adding or removing capacitance or inductance is as much of an art as a solid mathematical process. The equations representing the change of network impedance, when introducing different electrical components, are shown later. The Smith chart, shown in Figure 3.5, is a tool, used with the equations discussed next, to determine what capacitor or inductor should be inserted in to the matching network and where and where to insert them.

The network analyzer can display the impedance of a load on the Smith chart as a frequency dependent function. The line shown in the Smith chart in Figure 3.6 is the impedance in the frequency range specified. The network analyzer can be used to determine the impedance at a desired frequency to be matched. The components in a matching network can be chosen given known impedance, which can be measured from a network analyzer, with

$$L = \frac{Z_0(X_j)}{2\omega j} \quad C = \frac{-j}{\omega(X_j)Z_0} \tag{3.2}$$

where C is the capacitance value for an added capacitor, L is the inductance value of an added inductor, Z_o is the network impedance, and X_j is the reactance of the network. Once the network was matched, the signal at the selected frequency was created using the Agilent function generator run through the amplifier. The signal was sent through a dual-directional coupler and monitored via an Agilent N9320A Spectrum Analyzer to measure the forward power and the reflection back into the amplifier.

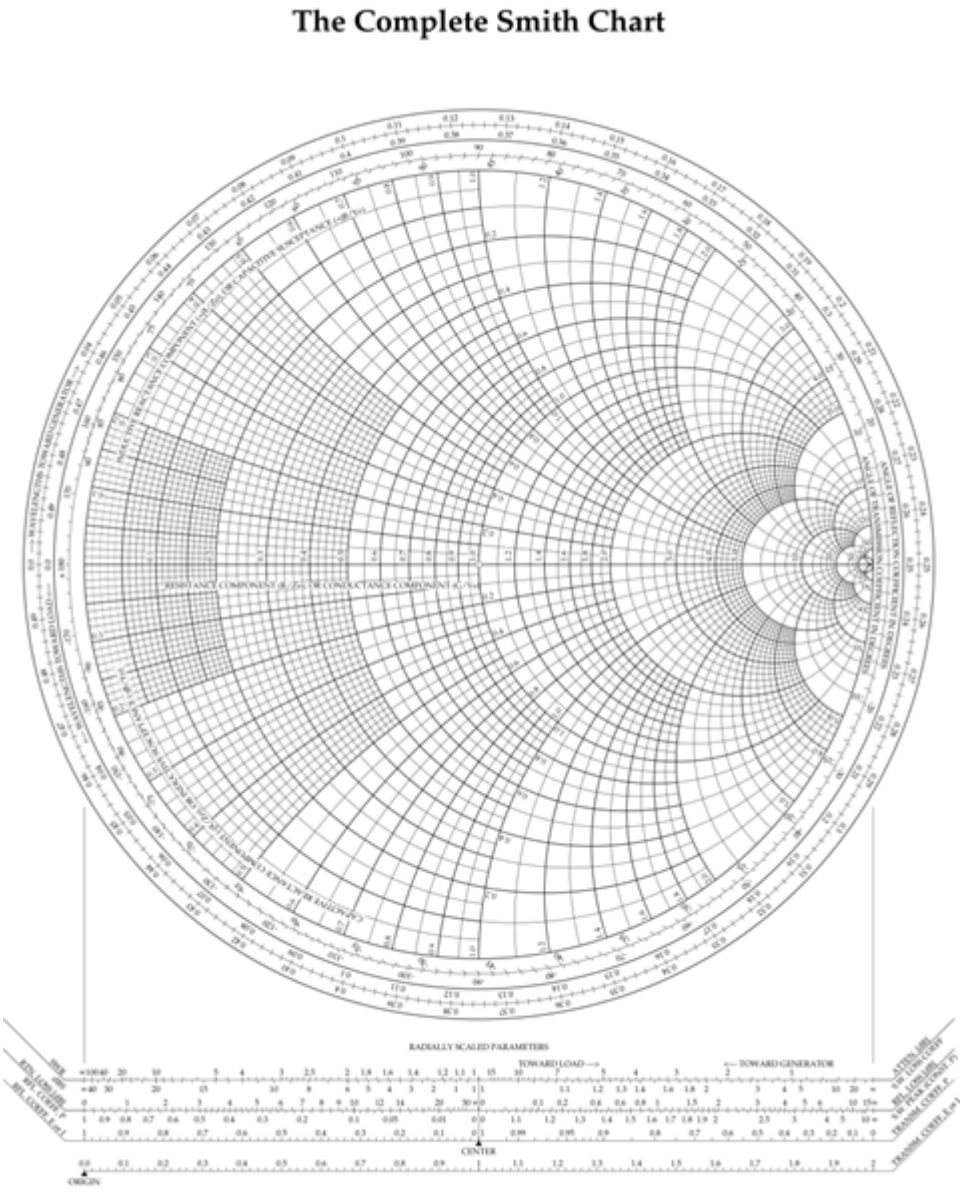

Figure 3.6: The Smith Chart

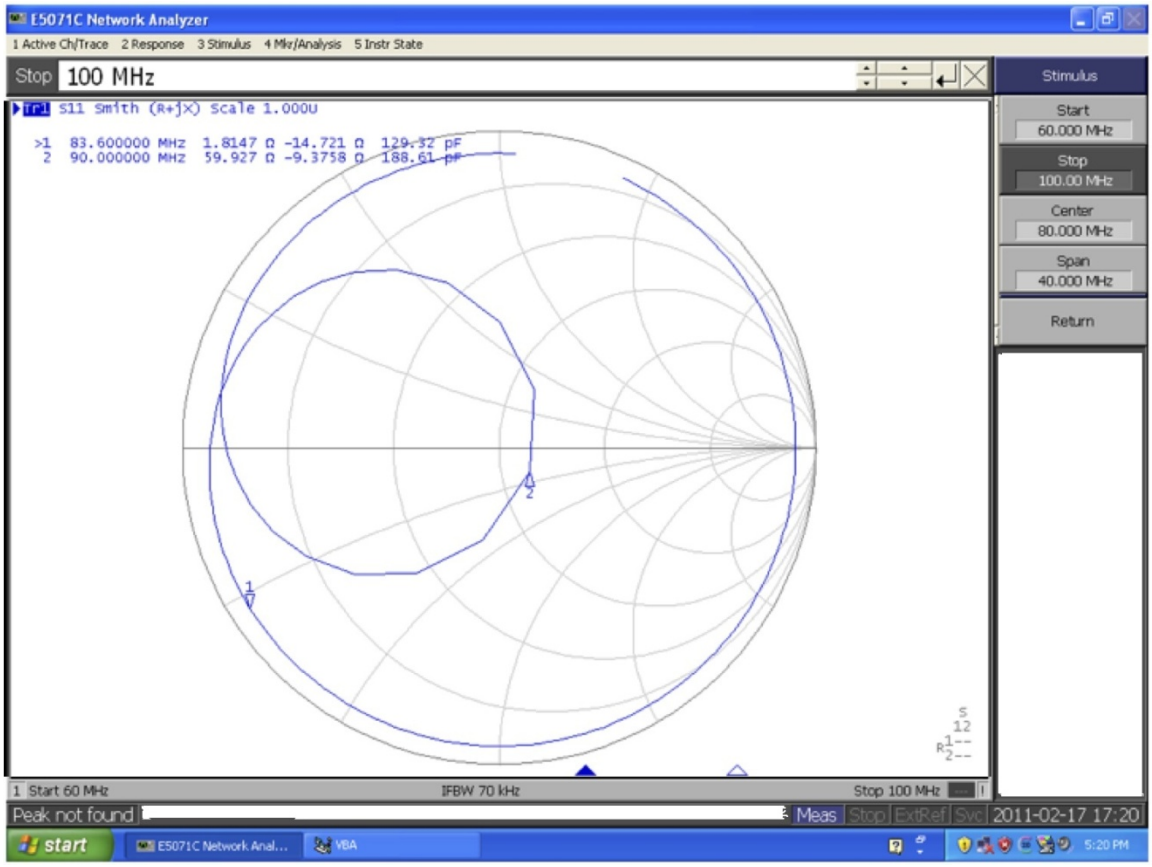

Figure 3.5: Network Analyzer Using Smith Chart for Matching

3.4 Electric Field Mapping

Mapping the test area to understand the RF radiation pattern and correlate the RF field to transport measurements is important for understanding the stimulating mechanisms. The EM field was mapped in the test region using a three dimensional computer controlled translation-table, which was used to move a probe connected to the spectrum analyzer to nodes of a desired 3D grid. By probing the medium and recording the measurements, a three dimensional map of the field was constructed. The three-axis positioner was built using an aluminum frame, stepper motors, and ball screws for positioning. The mechanical and electrical components were designed and were built in house.

The frame of the tri-axial positioner was built of a t-slotted aluminum frame made of "80/20" brand material, which is joined with plates using bolts. There are metal tracks for the tool fixture to travel linearly in the three axes. Three stepper motors turning ball screws, which provide accurate translation of the aperture, enable precise and consistent positioning. The three stepper motors, a controller network, and drivers were all acquired from Keling Inc. The tool fixture consists of an aluminum plate with two clamps for attaching the antenna. The clamps secure the glass tube containing the probe, to provide rigidity and waterproofing. The probe is constructed of a 3.5-mm coaxial wire with a solid copper outer shield. 2.5 cm of the outer shield is stripped creating the input antenna, which is connected to the spectrum analyzer through an 18-GHz precision test cable. The 18GHz cable is constructed with an N-type male connector at the spectrum analyzer connection and a SMA male connector on the probe end.

A controlling code, developed in LabView software, controls the three stepper motors through the control box. The program is written to move the probe in three directions in incremental moves according to a tab-delineated text script written for the desired path, which are either depth (vertical) and/or cross-sectional (horizontal) slices. The probing to map the field was conducted on a 2-cm grid in the areas of the test medium that do not interfere with the antenna, support table, and upper supports for the antenna and dye injection pipette.

To move the positioner to a designated measurement location, a path script was written using Microsoft Excel and then exported to a tab-delimited file. The script consists of three columns relating to the three Cartesian coordinates X, Y, and Z location of the probing node. To minimize errors, the path moves to each (X, Y) coordinate and then completes all moves on the Z-axis correlating to that point in the X-Y plane. The probe stops for 2 seconds to take a measurement, allowing the spectrum analyzer to acquire a steady and consistent reading. Readings, collected using the spectrum analyzer at each point, are exported to a tab-delimited 4-column text file, corresponding to X, Y, Z, and the power measurement.

The measurements were the peak power, as recorded by the spectrum analyzer at the frequency of the signal. Readings were recorded in power (dBm) and were easily distinguished by using the programs “peak value” function because the peak values were magnitudes above the background noise. The spectrum analyzer was controlled remotely by a LabView program and set to a range of available frequencies of 50 MHz to 200MHz, which is the limitation of the equipment.

3.5 Imaging

Digital imaging was used to analyze the transport of dye and determine the stimulation effect. Taking images at consistent time intervals and using the images to measure dye concentrations, enables the determination of the transport rate.

Images were taken with a Cannon Rebel T2i 18-megapixel digital camera. The images were captured using an EFS 18-55mm lens, zoomed to encompass the entire testing medium. To ensure consistent and stable images, a tripod supported the camera. To actuate the camera and minimize vibrations, a remote capture program was used to control and download images.

Canon's EOS software package, specifically the Remote Capture function, was used to capture the images at designated intervals. The images were downloaded directly to the computer through the remote capture program and could be managed and accessed easily. Images could be taken a range of intervals but were taken at 1-minute intervals for this experiment. Images at a 1-minute interval give enough information without capturing and managing a large number of data files.

For our purposes, the Manual mode setting on the camera was used to enable control of more of the camera settings. Using the camera manual mode enabled choosing the shutter speed, aperture, ISO (image sensor sensitivity), and image format. The images were taken in the RAW format to maintain the highest level of information. A shutter speed of 1/40 sec, an aperture setting of F13, and ISO of 800, produces the best result with the lighting conditions that were created with the apparatus. The auto-focus mode was found to be consistent and accurate and was, therefore, used for this experiment.

The lighting of the test medium was very important to the analysis of the diffusion. The images were taken opposite the light source, which enables measuring the dye through light transmission-mode. To ensure a uniformly lit background, a light box was built along with a diffusive filter. The light box consists of a wooden frame built out of 2" × 4" fir attached to a 12.7-mm (½ inch) plywood backing. Three florescent tube lights 60.96cm (2') long are attached to the inside and back of the box. To diffuse the light, white Lycra is stretched across the opening of the box. To diffuse the light further and to create a more uniform backlight for the apparatus, a second frame made with white Lycra was used. These two layers of Lycra were spaced approximately 20cm apart to diffuse the light enough to reduce drastic backlight gradients to an acceptable level although not enough to completely eliminate variations in intensity. The pixel values of the 2D digital images correlate to the integral of the dye concentration along the line of sight. The images were broken down into a matrix, which could be manipulated to determine the properties of the dye transport.

4 SUMMARY OF RESULTS AND DISCUSSION

Several tests were performed to develop the methodology described in this thesis. The data presented in this section resulted from the final methods developed. The thermal tests were very early on in the investigation and are considered a separate series not in the same apparatus as the EM stimulated tests. The EM stimulated tests used for this data consisted of two runs at each power of 50 Watts, 30 Watts, 10 Watts, and 0 Watts. Each run consisted of 130 digital images, 10 background images and 120 data images. The background images were used for subtraction that will be discussed in Section 4.2. The effects of the stimulation are shown to be dependent on the antenna configuration and orientation. The EM field was mapped in depth slices so that the results can be viewed in a two dimensional format.

4.1 Thermal Tests

The thermal tests were performed to compare the stimulating effects of temperature and EM waves on diffusion as well as to minimize and to monitor the temperature change during EM stimulation. The relationship between diffusion and temperature was observed to be logarithmic; as the temperature is increased, the diffusion rate increases proportionally to the log of the time. Figure 4.1 shows the relationship between temperature and the inverse of the time required to reach steady state (uniform

concentration). The temperature versus the natural log of the inverse of time required to reach a uniformly diffused concentration is also shown in Figure 4.1.

Figure 4.1 shows the results from the experimental setup described in Section 3.1, the increase of the diffusion rate due to thermal stimulation. The time to reach a steady-state condition (uniformly diffused concentration) is proportional to the diffusion rate and so is used for the comparison. The natural log of the diffusion rate is linearly proportional to the temperature, so the relationship is logarithmic. Although thermal effects were important to observe and to account for, there was no significant heating recorded in the EM diffusion tests.

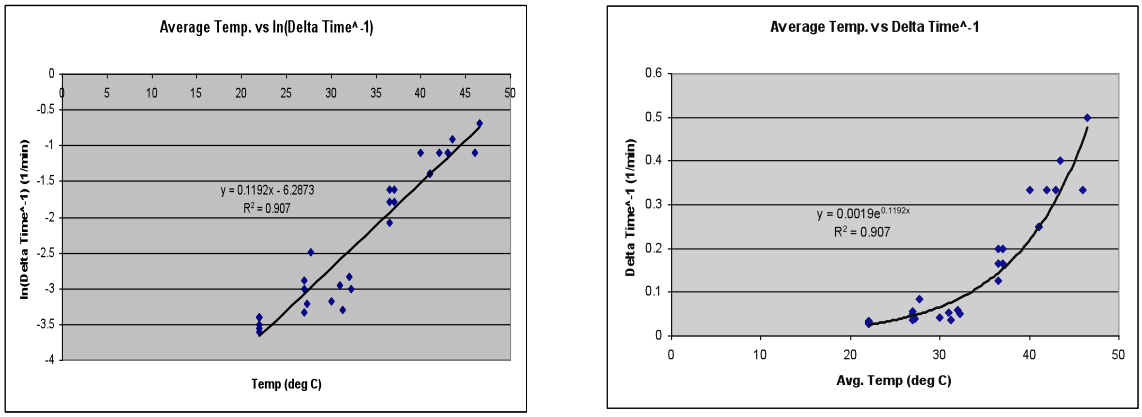

Figure 4.1: Relationship between temperature and the time required to reach steady state: Linear-scale (Left); Log-scale (Right)

4.2 EM-Stimulated Tests

4.2.1 Creating Reproducible Dye Injection

Initial tests were performed to determine if there was an effect on the diffusion due to the EM stimulation. Hence, this process needs to be repeatable and requires a reproducible dye injection method. These tests were recorded with digital images for comparison. The diffusion without stimulation is fairly horizontally symmetric about the

injection area. Figure 4.2 shows the non-stimulated diffusion pattern where the dye descends vertically from the injection table and spreads in all directions along the bottom of the tank and up the sides.

Originally, the antenna was positioned vertically in the CPVC pipe and box. The stimulation from the vertically polarized antenna created a focused transport pattern very similar to a vertical advective flow. Monitoring the flow of water shows no advection. The antenna was placed horizontally to evaluate the effect of radiation pattern on the stimulation and flow. The horizontal antenna creates a very consistent effect that can be easily captured with digital images.

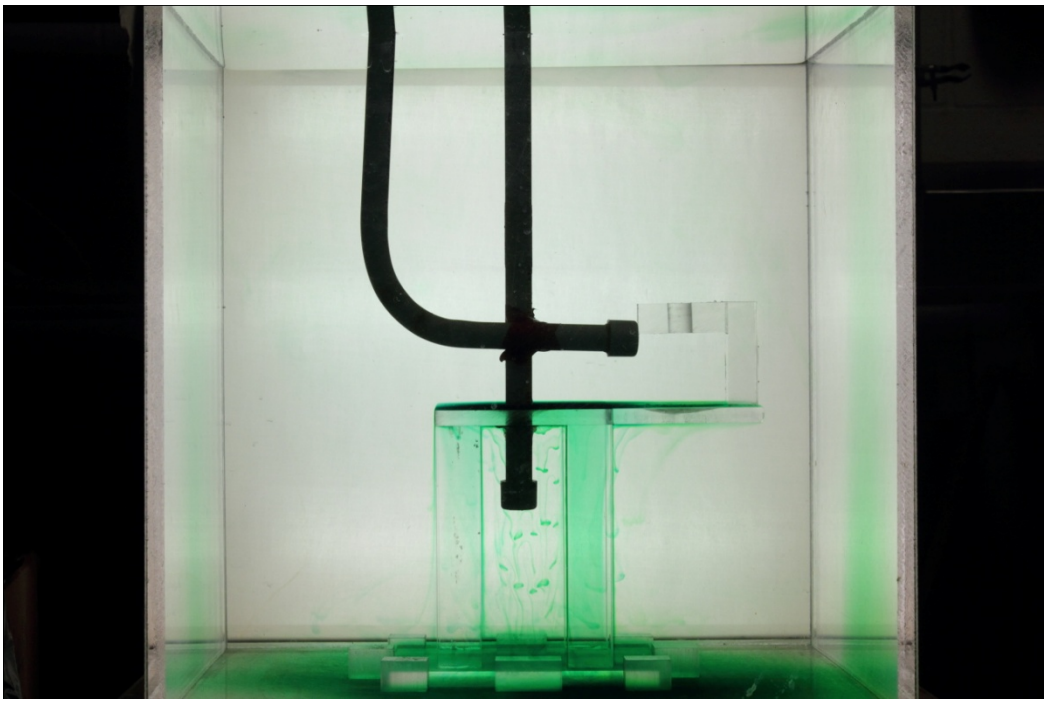

Figure 4.2: Non-Stimulated Diffusion Pattern

The first stimulating source used a PVC-cased vertically-polarized monopole antenna (made of a co-axial cable). The stimulated transport pattern, for this antenna configuration with 50 Watts of Power at 153MHz, has the dye moving up the PVC pipe to the surface of the water and dispersing from the pipe as seen in Figure 4.3.

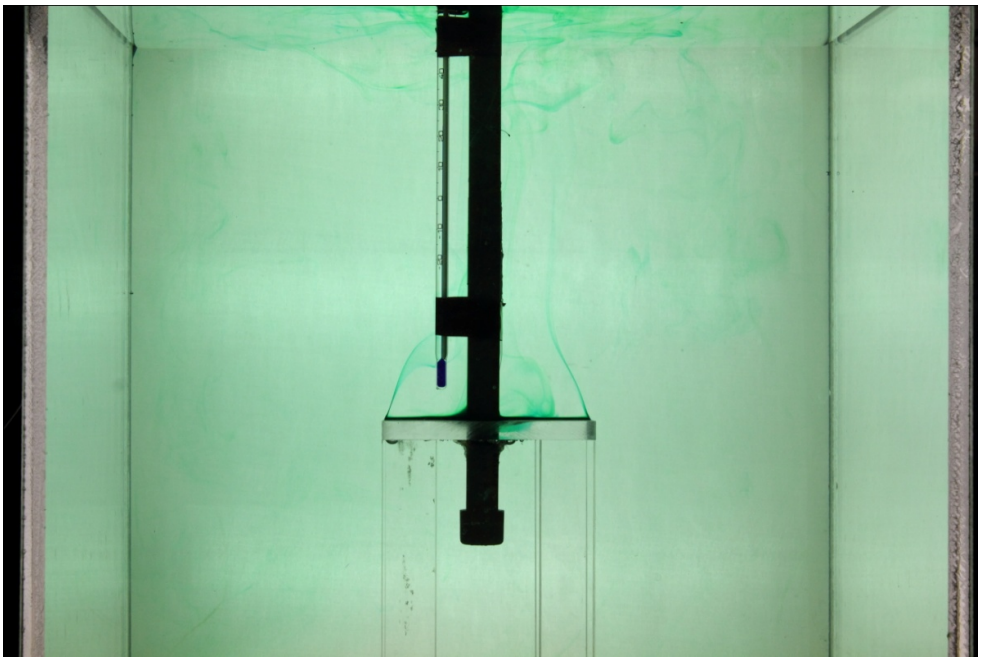

Figure 4.3: Stimulated with vertically-polarized CPVC-cased monopole antenna, thermometer spaced off CPVC

In Figure 4.3, the dye is moving in an upward trend and dispersing at the surface of the water. As seen in the figure, a thermometer is placed close to the CPVC-cased antenna to measure any change in the temperature. No measurable temperature change was recorded. In Figure 4.4, the thermometer was moved closer to the CPVC pipe to measure any temperature changes in the vicinity of the antenna. Again because, no measureable temperature change was observed, convective flow due to thermal gradients was determined to be minimal.

Further tests were needed to show that the effect on the dye movement and diffusion were the result of the stimulation. The next step was to inject the dye away from the antenna to make sure that no attractive mechanism between the body of the antenna casing (CPVC) and dye existed, even though there was no obvious potential mechanism. A dye cup and holder was built to space the injecting pipette away from the antenna,

which can be seen in Figure 4.5. These tests were referred to as spaced injection tests and were conducted with 50 Watts of stimulating power at 154 MHz.

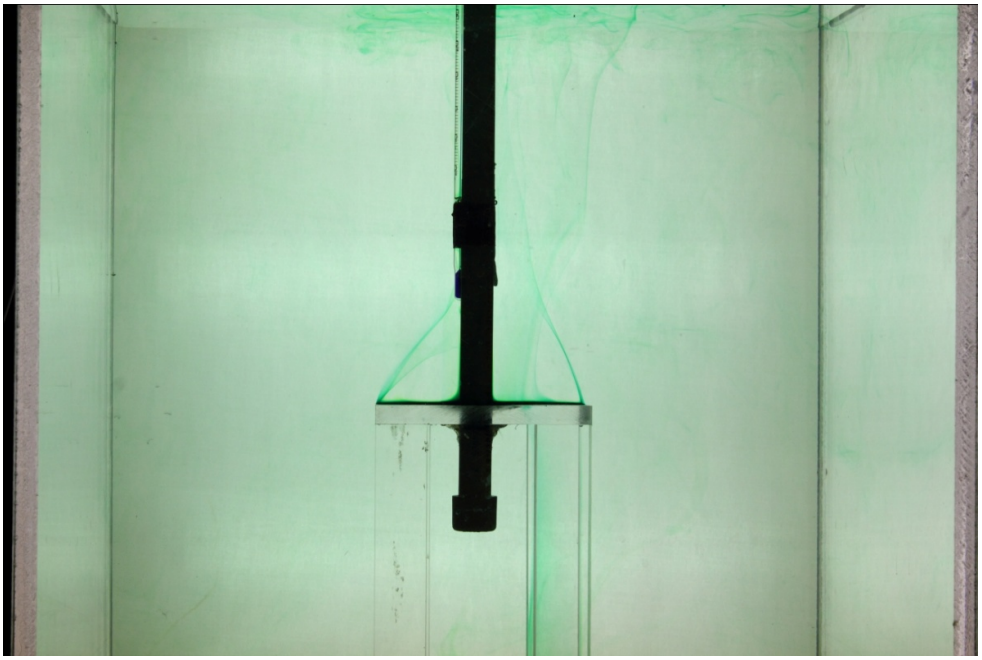

Figure 4.4: Stimulated with vertically-polarized CPVC-cased monopole antenna, thermometer shown on left

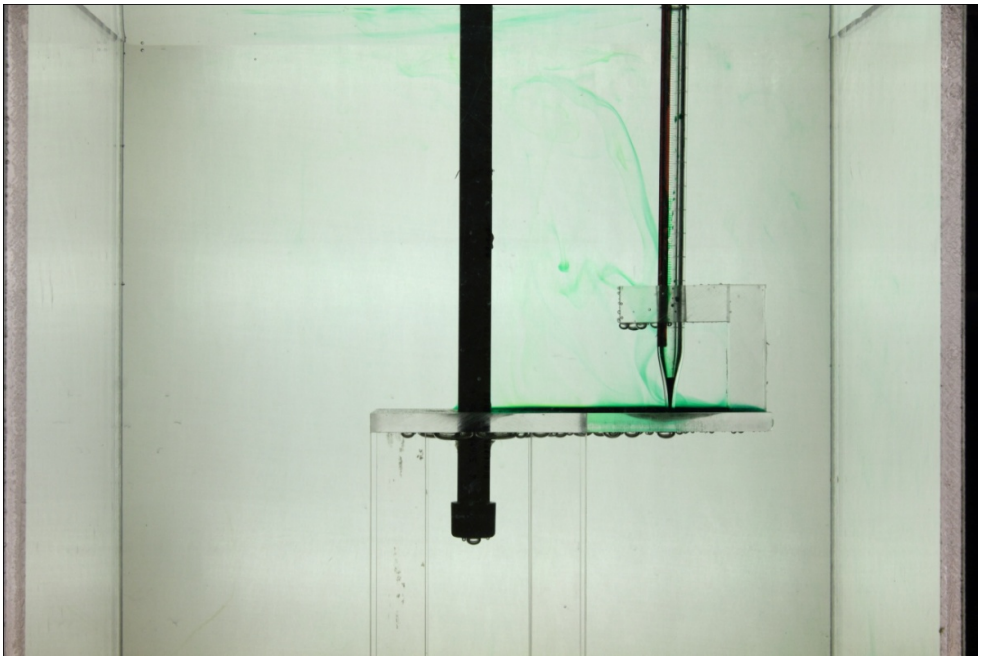

Figure 4.5: Stimulated Spaced Injection Test

Again, the dye moves up the CPVC casing and toward the surface to disperse. Fingering away from the pool of dye diffused toward the antenna and surface, similar to fingering in the non-spaced injection case. This diffusion pattern again could not be attributed to thermal effects, since no measureable temperature changes were recorded. Since any minimal thermal gradient could cause a convective flow and to distinguish a convective flow due to EM-heating and direct stimulating effect from the EM waves, the radiation pattern on the electric field needed to be altered, and the transport pattern needed to be monitored as the next step.

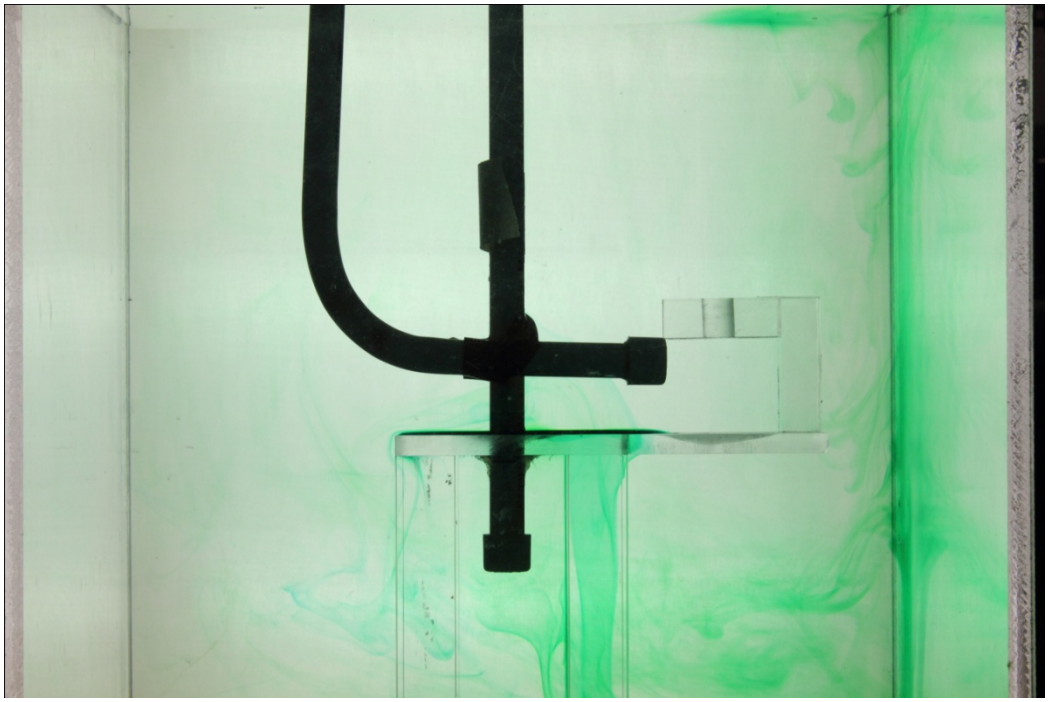

Figure 4.6: Stimulation with horizontally-polarized monopole antenna

To demonstrate that the changes in diffusion were the result of EM stimulation, we changed the antenna position and configuration to create a different field within the test medium. Figure 4.6 shows the profile of the CPVC-cased monopole antenna in a horizontal position. This horizontally polarized monopole antenna has a totally different radiation pattern. Since the dye moves downward first and in a pattern following the

antenna direction, the effects on the diffusion pattern are clearly not the result of thermal effects near the antenna. This test again used 50 Watts of stimulating power at 154 MHz.

Figure 4.6 shows diffusing dye to the right of the testing medium with very little dye diffusing to the left. The contrast in the diffusion pattern shows the clear effect of the EM stimulation and the radiation pattern of the antenna on the diffusion of the dye in water. The tests shown in Figures 4.2 through 4.6 were repeated and showed strong consistency. This series of tests clearly verify the effect of the EM-stimulation and the radiation pattern on the dye diffusion.

To fully analyze and observe the effect on transport, the entire water medium was captured in all future images. The flow in the non-stimulated case shows resemblance to diffusion. However, because of the uncertainty of the flow mechanism in the EM-stimulated case, the general term "transport" is used to address the transport of the dye. By imaging the entire medium, the transport of the dye throughout the confining area can be visualized. To ensure no mechanism or random factor (e.g., non-level injection table) other than the RF electric field affected the transport, the acrylic box and entire setup except the EM-source was rotated 90^{o} around the injection area. This rotation still resulted in a consistent transport pattern, confirming the field radiation pattern as the dominant factor affecting the transport (Figure 4.7). As seen in Figure 4.7 the majority of the dye transports in a pattern that were mirrored when the antenna rotated 180^{o}. In two dimensions it is hard to see that in each test the dye would move to the wall that the antenna was pointing toward, similar to what is seen in Figure 4.6

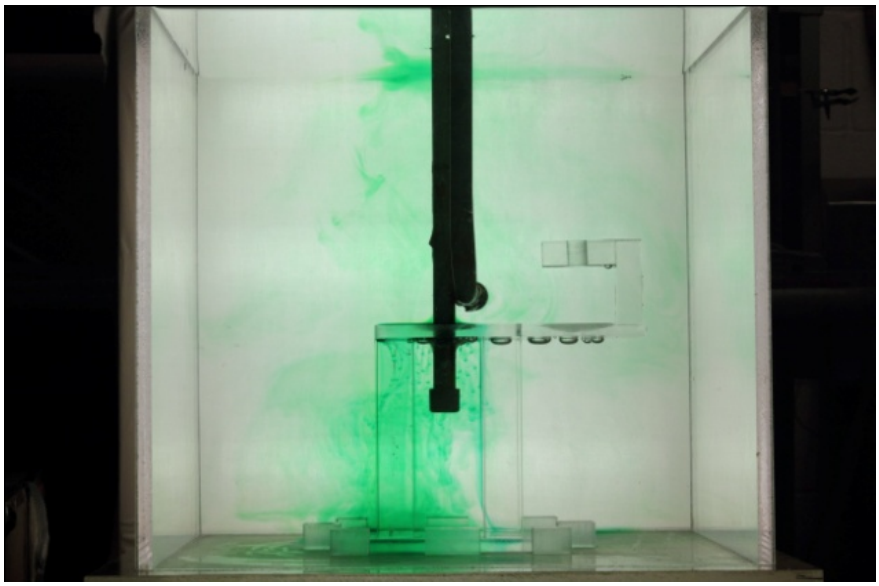

(a)

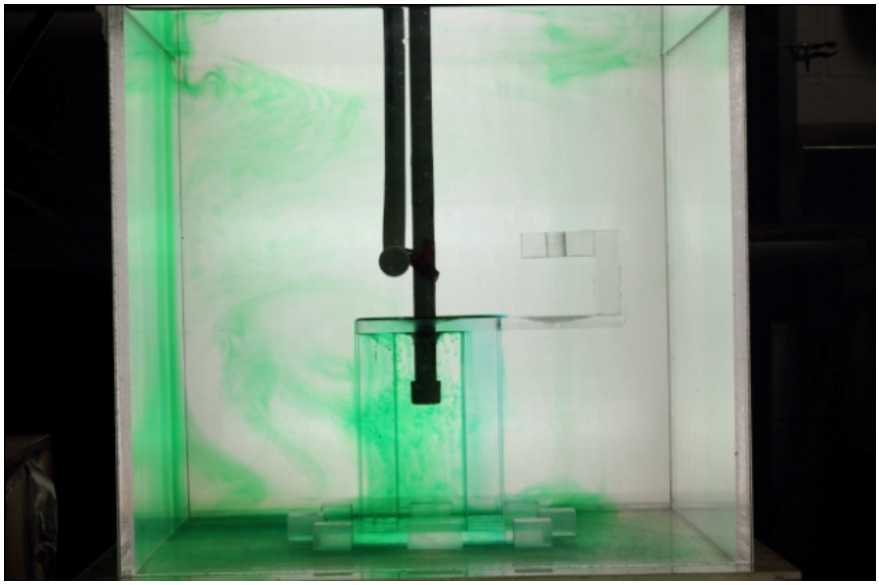

(b)

Figure 4.7: Stimulated diffusion with: (a) Antenna turned away from the camera (left, back view); and (b) Antenna toward the camera (right, front view)

Although the diffusion patterns shown in Figure 4.7 are repeatable, it is determined that the horizontal antenna oriented perpendicular to the image provides the best opportunity to quantify the changes in the dye transport pattern from EM

stimulation. The following tests results were all obtained with a horizontally-polarized antenna. There were a series of tests consisting of two tests at 50 Watts, 30 Watts, 10 Watts, and 0 Watts at a frequency of 154 MHz. A typical diffusion pattern created by 50 Watts of stimulation is shown in Figure 4.8.

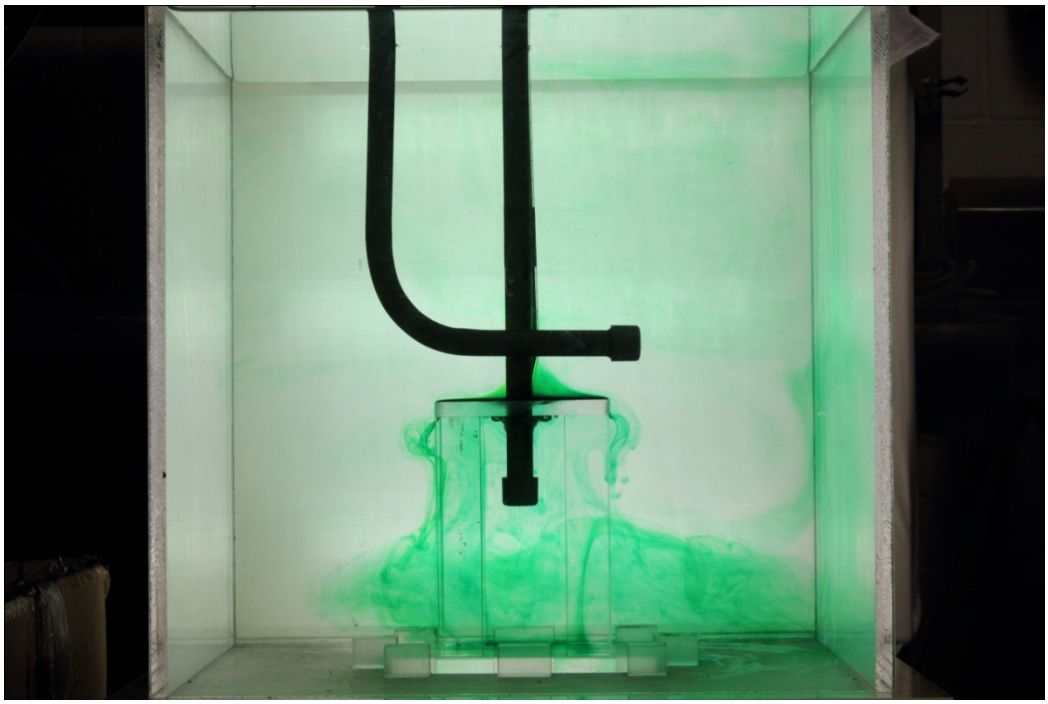

Figure 4.8: 50 watt typical diffusion pattern (side view)

4.2.2 Field Mapping

To fully analyze the stimulation and its effects, the radiation pattern and electric field within the testing medium need to be mapped. The field probing technique described in Section 3.5 (Mapping Electric Field) enables construction of a map of the RF electric field, antenna radiation pattern. The output of the LabView program (described in Section 3.5) collecting the electric field measurements is a 4-column tab-delimited file. An example of the LabView output file from a typical depth slice is shown in Figure 4.9.

-12	-10	0	8.241
-12	-10	2	7.856
-12	-10	4	7.027
-12	-10	6	5.111
-12	-10	8	2.535
-12	-10	10	-0.921
-12	-10	12	-6.092
-10	-10	12	-5.43
-10	-10	10	-1.277
-10	-10	8	1.773
-10	-10	6	3.872
-10	-10	4	5.361
-10	-10	2	6.59
-10	-10	0	7.327

Figure 4.9: LabView data from ENF10. Columns from left to right are: X, Y, Z, and Power in dBm

These columns represent the Cartesian coordinates of probing point (X, Y, Z) and the power reading (dBm) at that point, respectively. The second column corresponding to Y shows one value in this example, since this is from the depth slice of data taken at X= -10 cm (from the origin). The power data is in dBm, which is converted to a linear scale to represent the electric field in the following sections. The linear conversion of power was done by using Equation 4.1.

$$\left|E_{RF}\right| = \sqrt{10^3 \times 10^{\frac{Power(dBm)}{10}}} \tag{4.1}$$

The reverse log-transform and square root are used to convert the log-scale power reading to a linear electric field magnitude. Neither the power reading nor the electric field reading is calibrated, but they are normalized to between zero to one, corresponding to global minimum and maximum measurement. All values are positive.

The electric field maps shown are normalized to the global highest and lowest readings measured throughout all data taken. The data is normalized so that each field can be compared to another maintaining the same relative scale. The electric field maps shown are two-dimensional measurements taken as slices from the test medium. Figure

4.10 shows a schematic of the location of ten selected depth slices of the medium. The actual mapping on these slices will be shown following.

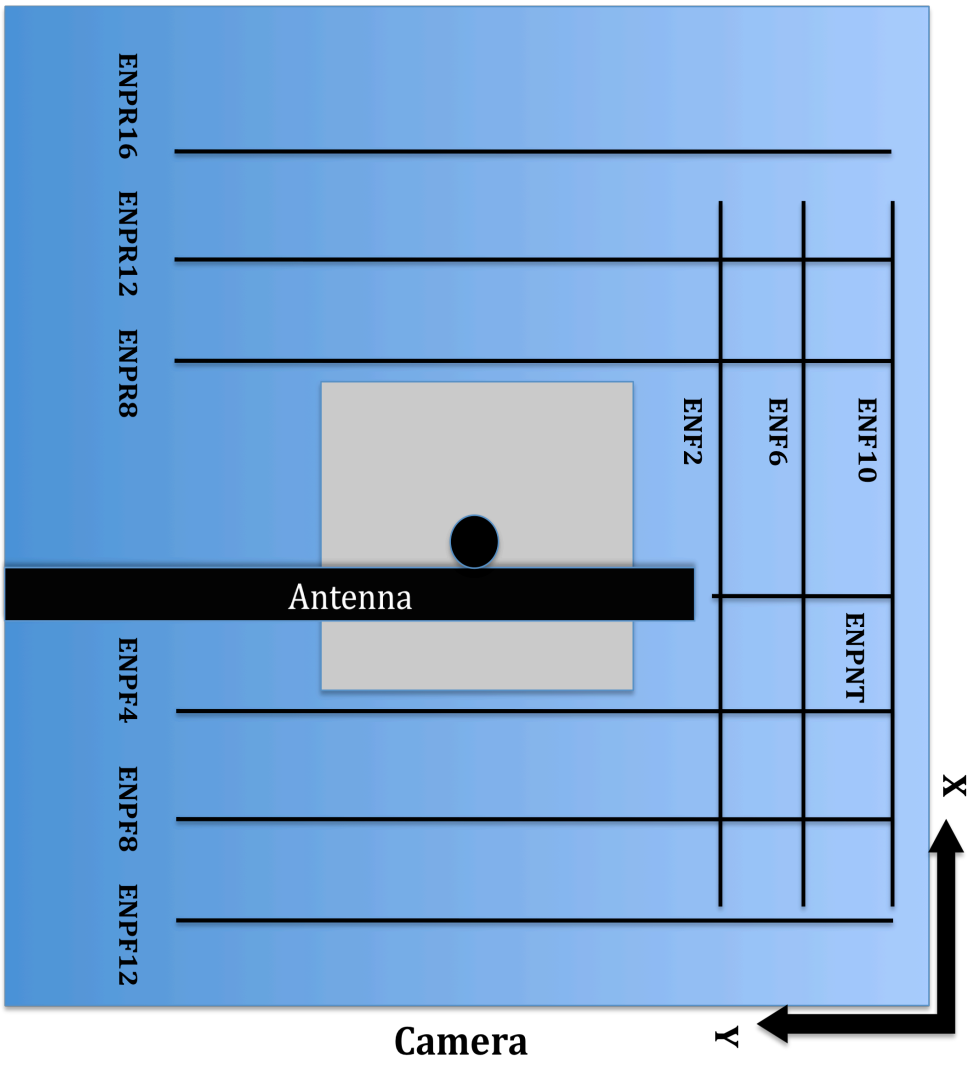

Figure 4.10: Schematic of Field Mapping Depth Slices Locations (top view of setup)

The data on these slices are all 25 cm in depth with the antenna centered at 12 cm from the bottom of each image (Z direction). Each slice is labeled to reference in the following images. An explanation of the labeling system is later in this section. The axes labeled in the upper right corner correspond to the probing coordinates. All images are labeled with the correct dimensions and relative normalized electric field strength. The electric field is not calibrated to real field values but normalized as mentioned. The

reason is because no power meter was used and the reception of the probe is not calibrated. The antenna is not a point source, yet the coordinate of the probing point corresponds to the tip of the antenna. Figure 4.11 shows contour maps of the electric field amplitude on the corresponding depth slices described in Figure 4.10.

In all the field maps, it is clear that the highest intensity of the electric field is toward the bottom of the tank. Also, as the probing distance from the antenna increases, from 2 cm to 6 cm and then 10 cm, the intensity of the field decreases, but not as much as would be expected with a propagating wave. The field strength with a propagating wave should decrease with the distance from the antenna. With a standing wave pattern the field does not decrease radially away from the antenna. A standing wave pattern can be seen in the field maps, corresponding to the wavelength of the RF wave in the medium. The Faraday cage most likely causes this standing wave pattern instead of the propagating wave that might otherwise be expected.

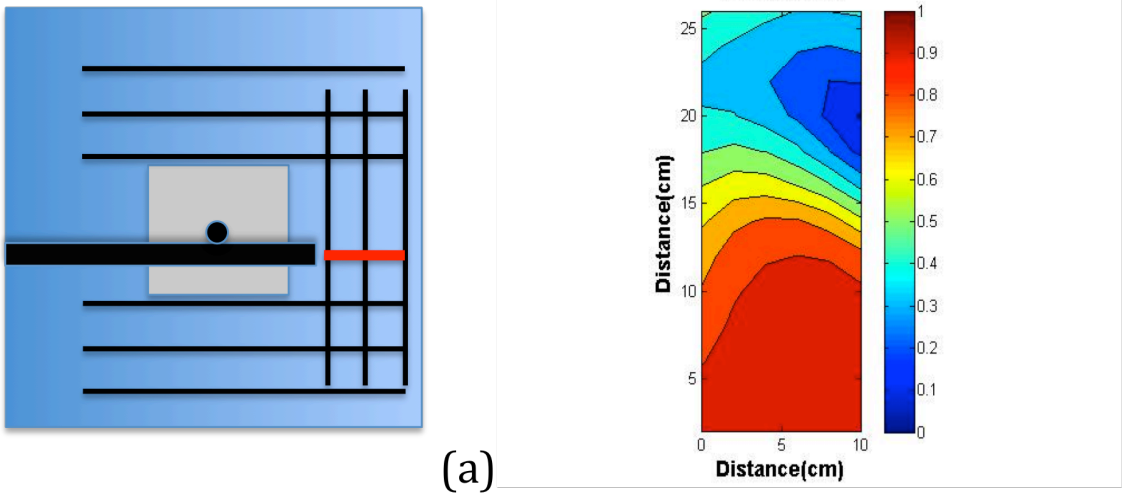

(a)

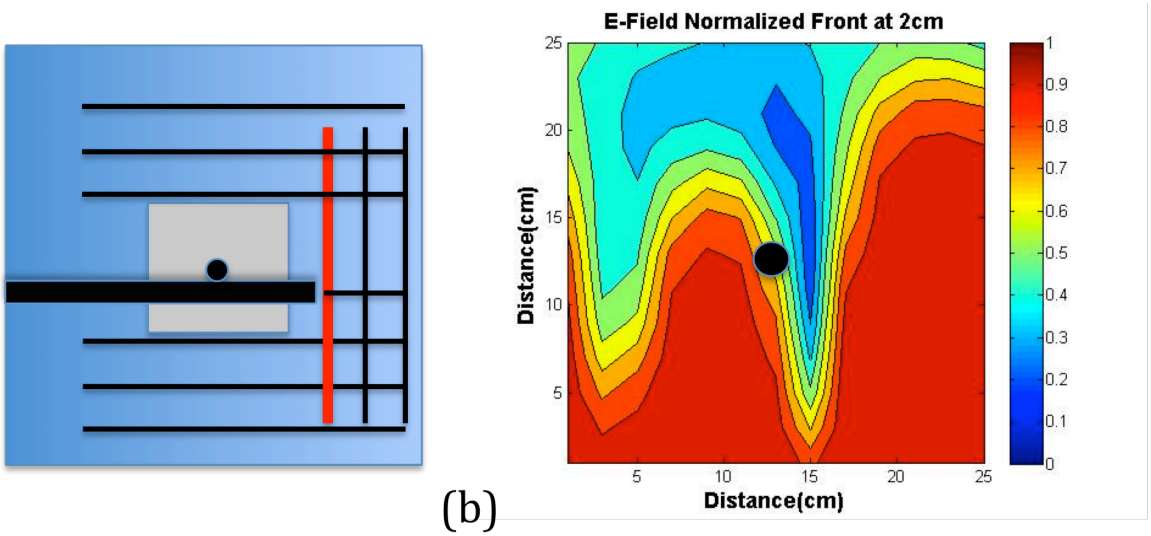

(b)

Figure 4.11: Depth Slice Electric Field Map of the Point Profile (a),

Front of antenna at 2cm (b), Front of antenna at 6cm (c), Front of antenna at 10cm (d)

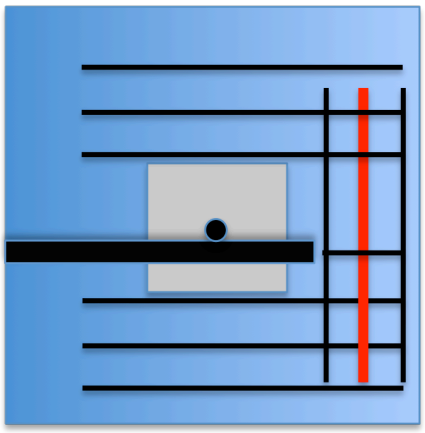

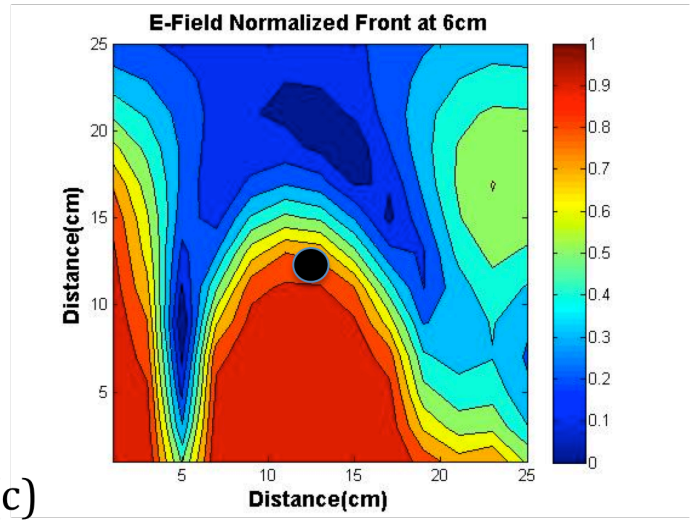

(c)

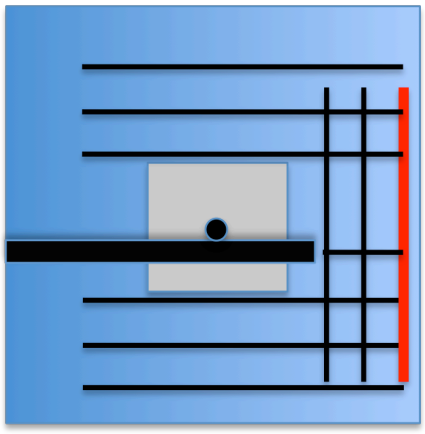

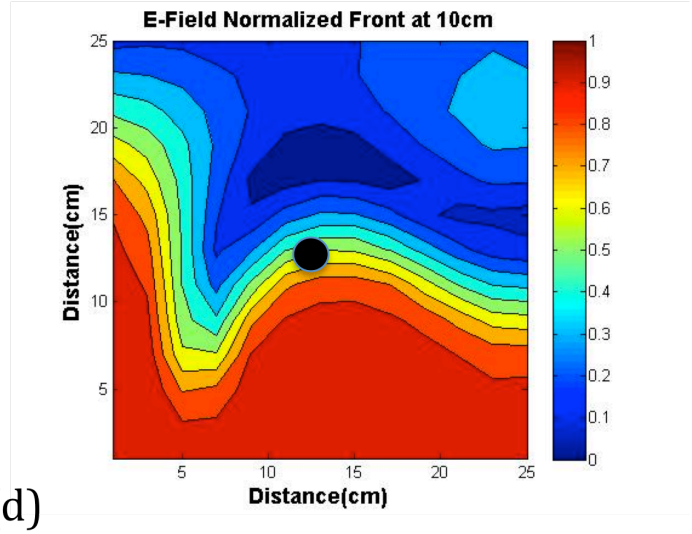

(d)

Figure 4.11 (continued): Depth Slice Electric Field Map of the Front of antenna at 6cm (c), Front of antenna at 10cm (d)

Figure 4.11 show the magnitude of the electric field and not its phase. The standing wave pattern that can be seen in the field profiles relates to the absolute intensity of the field in that plane of the medium. Analysis of the peak to peak or minimum to minimum of the RF wave pattern in the water medium shows that the half wavelength measures between 10 cm and 13 cm. Remember that a standing wave pattern has the peak to peak separation of ½ wavelengths. The full wavelength of these waves would then be between 20 cm and 26 cm. As mentioned, the wavelength of an RF wave is retarded by a value equal to the square root of the dielectric constant,

$$\lambda_{Water} = \frac{\lambda_{Air}}{\sqrt{\varepsilon_{r,water}}} \tag{4.2}$$

where λ_{Air} is the wavelength of EM waves in air; λ_{Water} is the wavelength of EM waves in water; and $\varepsilon_{r,\,Water}$ is the dielectric constant of water. At the emitted frequency of 154 MHz, the wavelength in air is approximately 194 cm. Assuming the dielectric permittivity of water is approximately equal to 81, the wavelength of EM waves in water will be approximately 21.6 cm. This result is consistent with the observations depicted in the field maps of Figure 4.11. The standing wave can be better seen in Figure 4.12, which are depth slices of the medium between the antenna and camera and behind, as described in Figure 4.10.

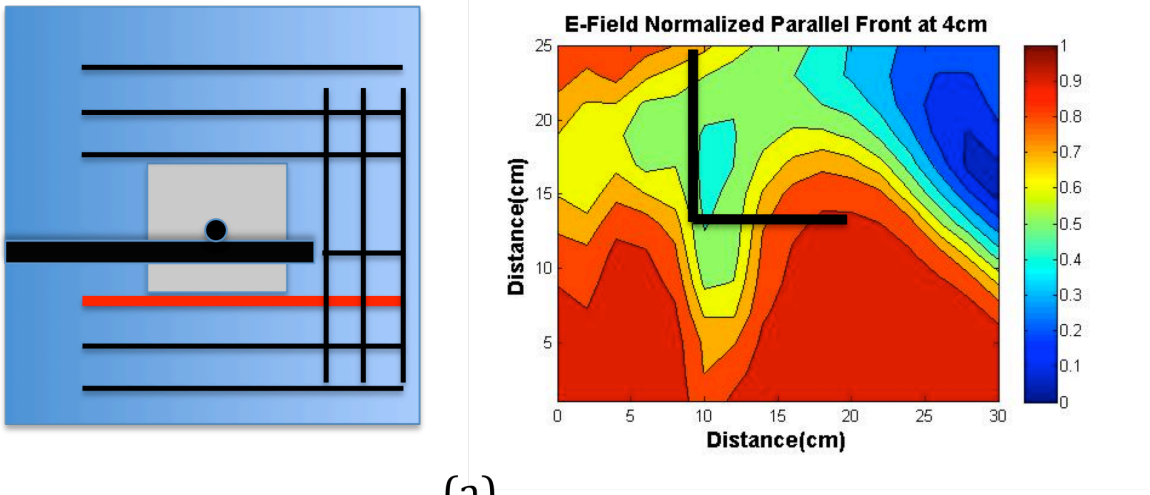

(a)

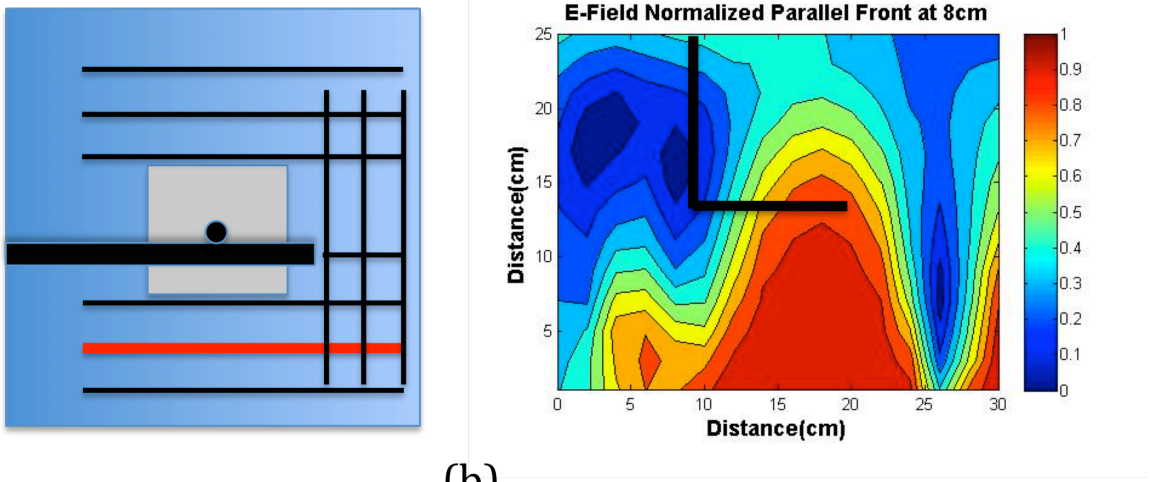

(b)

Figure 4.12: Depth Slice Electric Field Map of the Front Parallel to the Antenna spaced 4cm from center (a), Front Parallel to the Antenna spaced 8 cm from center (b), Front Parallel to the Antenna spaced 12cm from center (c), Rear Parallel to the Antenna spaced 8 cm from center (d), Rear Parallel to the Antenna spaced 12cm from center (e), Rear Parallel to the Antenna spaced 16 cm from center (f)

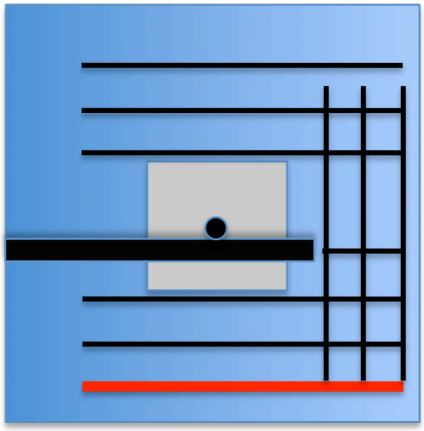

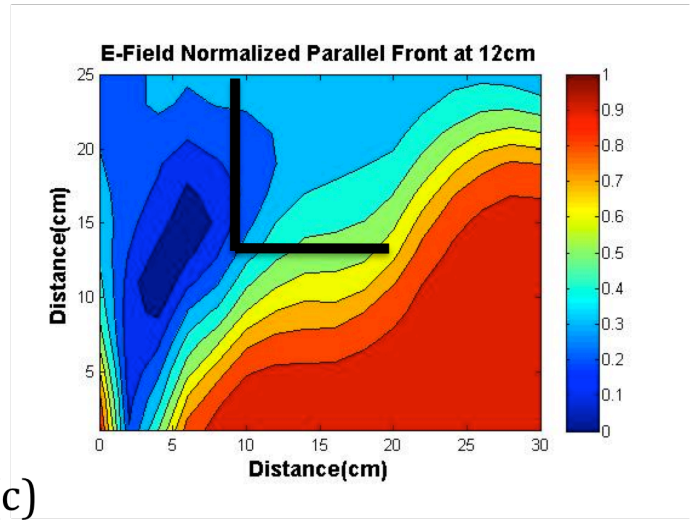

(c)

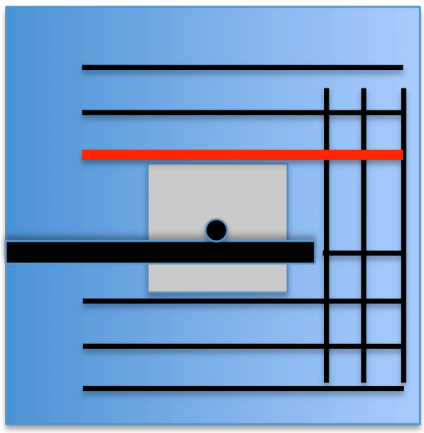

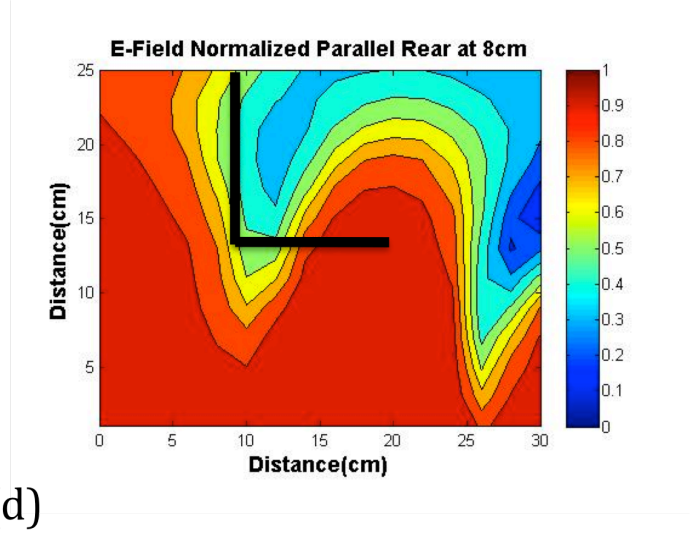

(d)

Figure 4.12 (continued): Depth Slice Electric Field Map of the Front Parallel to the Antenna spaced 12cm from center (c), Rear Parallel to the Antenna spaced 8 cm from center (d)

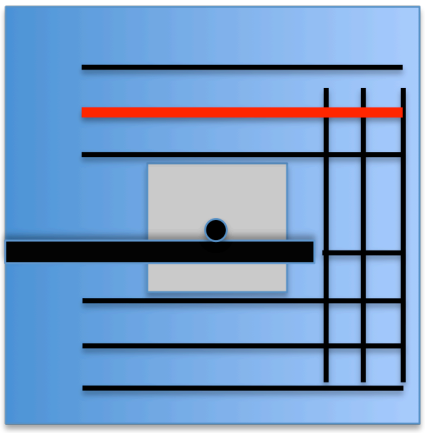

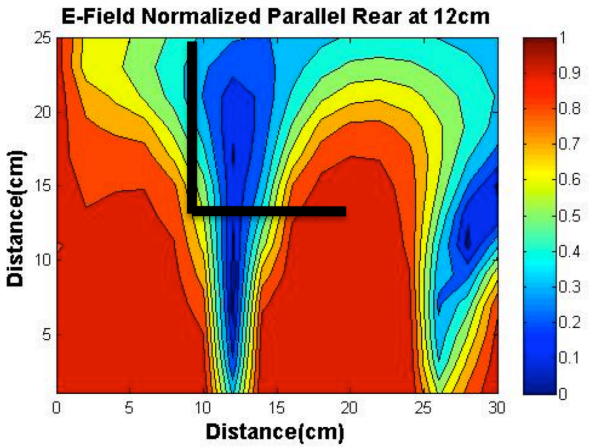

(e)

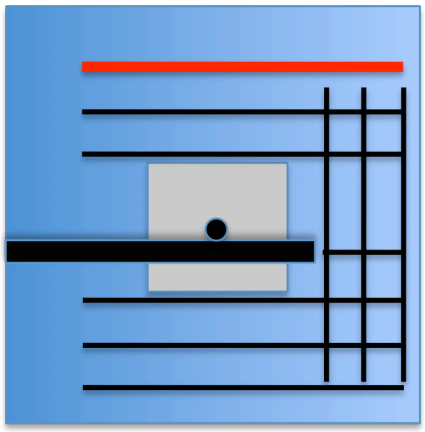

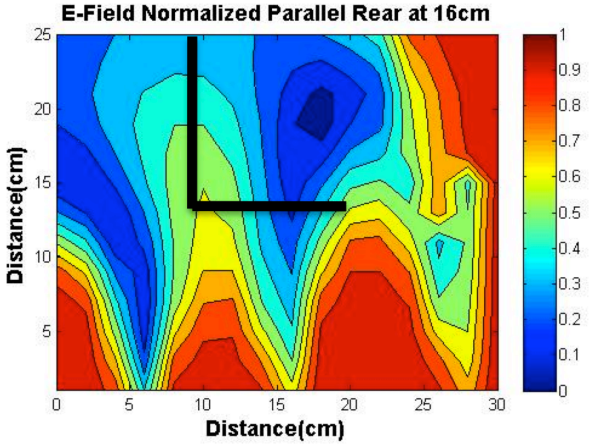

(f)

Figure 4.12 (continued): Depth Slice Electric Field Map of the Rear Parallel to the Antenna spaced 12cm from center (e), Rear Parallel to the Antenna spaced 16 cm from center (f)

In Figure 4.12, the standing wave pattern discussed earlier can be seen. The images (A)-(C) are of depth slices between the antenna and the camera, while (D)-(F) are from behind the antenna. It is important to note that in the images behind the antenna, a pattern more consistent with standing wave patterns can be seen. This difference between the front field pattern and the rear can be attributed to the large opening in the front panel of the Faraday cage toward the camera. Probing the field outside the water medium showed that there is little electric field outside, which allowed the large opening in the front panel of the Faraday cage. This partial cavity effect of the grounded cage is one reason behind the inconsistent field pattern of the front and the back of the medium. Despite this difference, the field is maximum at X = 20 cm (in the front zone of Figure 4.13) where the tip of the antenna is located.

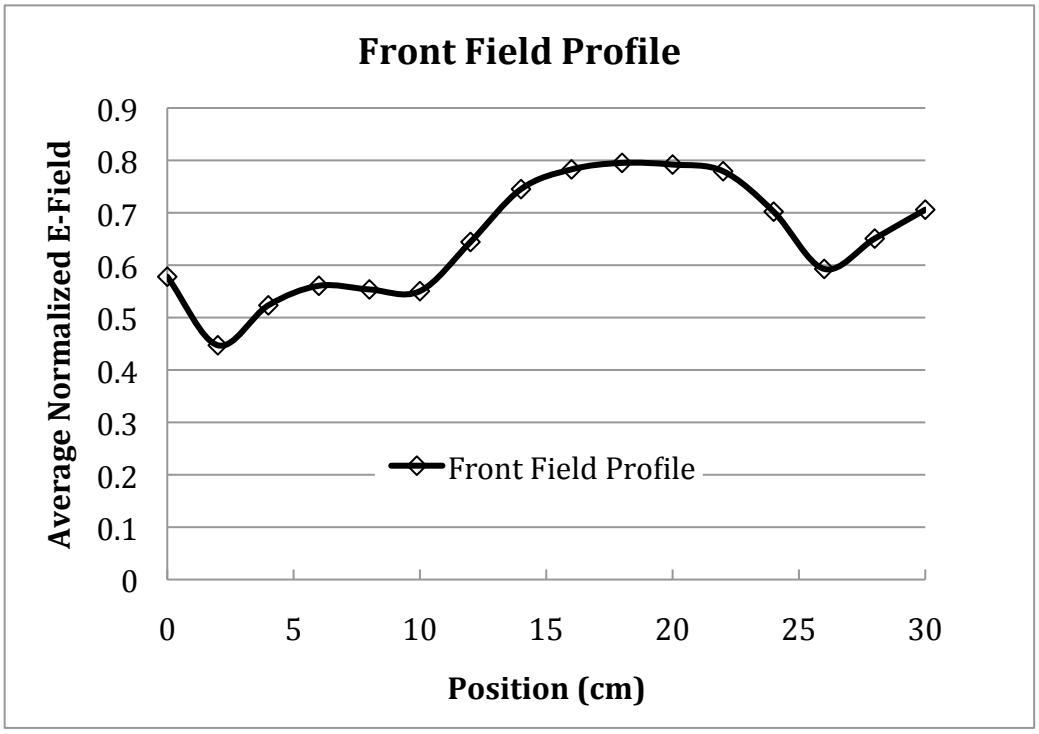

Figure 4.13: Front of box, normalized electric field (E-field) profile (between antenna and camera)

The electric-field profile, shown in Figure 4.13, clearly demonstrates the maximum field strength in line with the antenna and the field decreasing in strength away from the antenna, more so to the left. As can be seen in Figure 4.8, during stimulation the dye had a net flux toward the right side of the testing box. The extent of the difference in dye concentration between the left and right side of the images will be discussed in the following section.

4.2.3 EM Stimulation Effects

A MATLAB m-file program was written to compare and quantify the relative dye movement. The program integrates the amount of dye in different zones of the medium; the calibration will be discussed later in this chapter. The five zones that are used for comparison to determine the effect of the EM stimulation are shown in Figure 4.14.

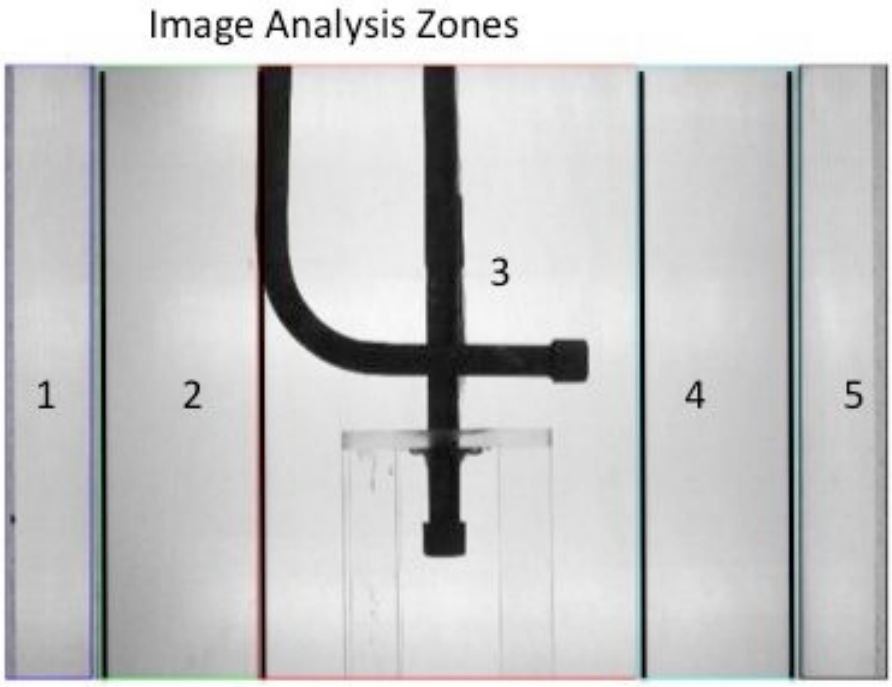

Figure 4.14: Zones 1 through 5 used for image analysis

Because the dye moved toward the right side of the testing box during EM-stimulation and had no apparent preferred path during non-stimulated tests, Zones 2 and 4 are compared and contrasted. Zones 1 and 5 had compounded error because of reflections at the water acrylic interface (i.e., left and right walls) in the box at the imaging angle. Therefore, Zones 2, 3, and 4 are used to compare the total amount of dye that has left the injection table. Although a very consistent amount of dye is injected onto the injection table, it leaves the injection table at different rates, so this is an important relationship to record. Before dye injection, ten images were taken and averaged to represent the background. This average background was subtracted from the remaining images, eliminating the water, the box, the antenna and everything but the dye for analysis. In certain areas, there is too much variation and noise caused by the apparatus, which is also removed from the image. The area that is removed or "masked" from analyses is the area around the injection and antenna pipes, the injection table, and the seams in the acrylic box, which is shown in Fig. 4.15 and indicated in black.

The vertical lines toward the left and right of the antenna are the seams in the box where distortions of color can occur. Once the background has been subtracted, leaving just the dye in the images, analysis of the dye can begin. A series of images are taken to calibrate the concentration of the dye. Calibration images were taken with known time increment, and hence, known incremental increases of concentration, which were used to calibrate the concentration in the stimulated and non-stimulated diffusion tests. A relationship between concentration and pixel value is established for a range of concentrations, but any pixel values above the calibrated concentrations are given the

maximum calibrated value. Assigning the maximum calibrated value will affect the results, but mostly during fingering of the dye. Once the finger has dispersed, the dye will reach a calibrated concentration and be recorded accurately. It is noteworthy that the calibration factor between image pixel values and dye concentration is spatially variable and nonlinearly dependent on the dye concentration. Both image pixel intensity and dye concentrations are integral values over the line of sight corresponding to each pixel. The calibration factor would also be different for different colors of red, blue, and green.

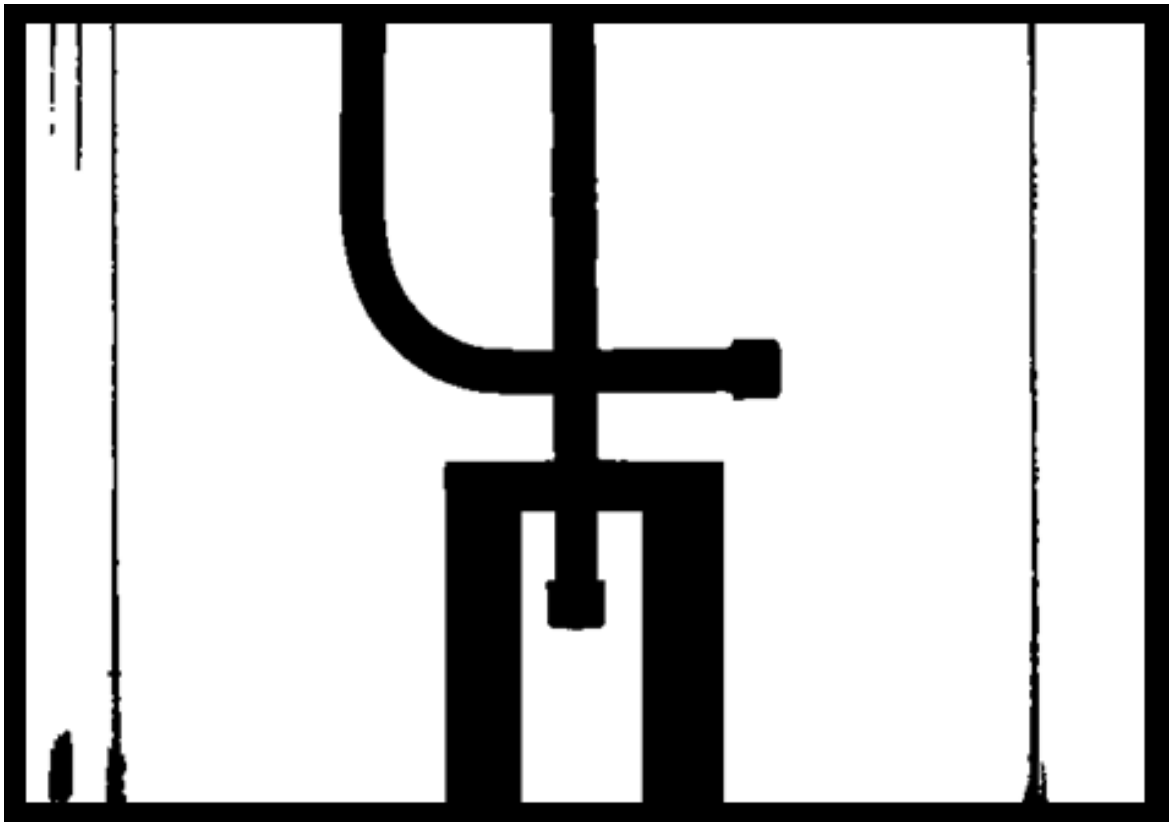

Figure 4.15: Area "masked" from analyses for removal of noise and variations due to apparatus

The images were separated into the three light spectra, red, blue, and green. In calibration, it is seen that the red and blue spectra are attenuated more with an increase in concentration, in contrast the green spectrum remains fairly constant. The green color in the images qualitatively appears more intense during imaging with high dye

concentrations. The green in the images appears to be more intense because of the attenuation of the blue and red spectra, leaving the green spectrum. The red and blue channels will be used to measure the dye concentration in this analysis because their intensity correlated to the dye concentration.

As seen in the earlier results, the dye transport would take a preferential path to the left during stimulation. To show the extent of this effect and to demonstrate the distinction with the non-stimulated tests, the results from Zones 2 and 4 are plotted. The graphs also show the blue and red separately for confirmation. In Figure 4.16, Zone 2 concentration, 50W-Z2R1, diverges from the Zone 4 concentration, 50W-Z4R1. 50W-Z4R1 is notation for 50-watt stimulated test, Zone 4 (as shown in Figure 4.12) and 1 indicates that this was run 1, out of 2 diffusion tests performed for 50-watt stimulation. The tests shown in Figure 4.16 through 4.19 are all of the same imaging zones, 2 and 4, during stimulation of 50, 30, 10, and 0 Watts at 154 MHz.

All tests start non-stimulated, and then EM-stimulation starts instantly. The spike seen in the Zone 2 plot marks the start of EM-stimulation in all images. There is a similar deviation shown in Figures 4.16 through 4.18, which are the concentration plots for 50, 30, and 10 Watts respectively.

The concentration in Zones 2 and 4 of the non-stimulated plot shows an increase at a similar rate throughout the test, as seen in Figure 4.19. The dye intensity in the 0 Watt or non-stimulated case shows that the dye concentration in Zones 2 and 4 rise together, diverging little other than temporarily due to dye fingering.

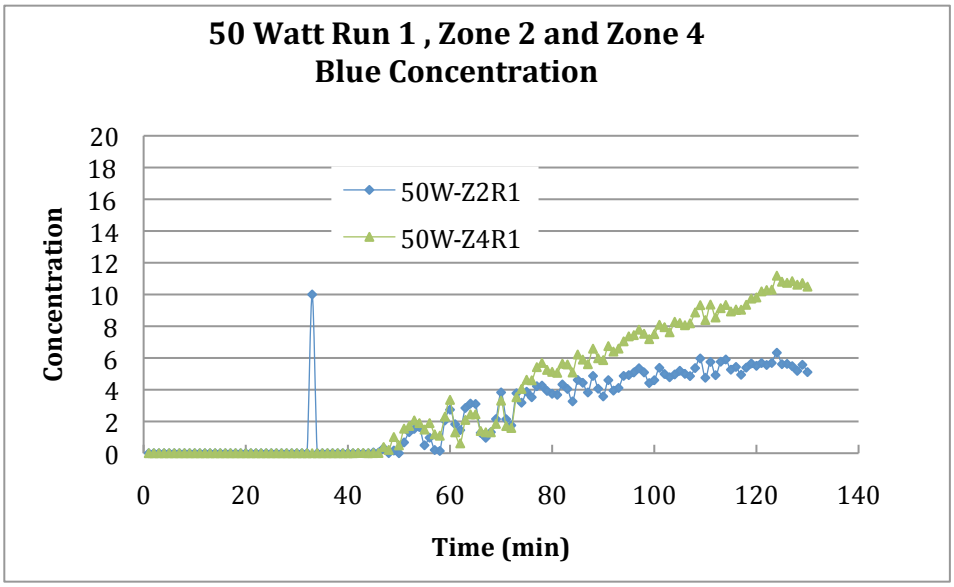

Figure 4.16: Zones 4 and 2, diverging concentrations in 50-Watt stimulated test. The spike indicates the start of stimulation

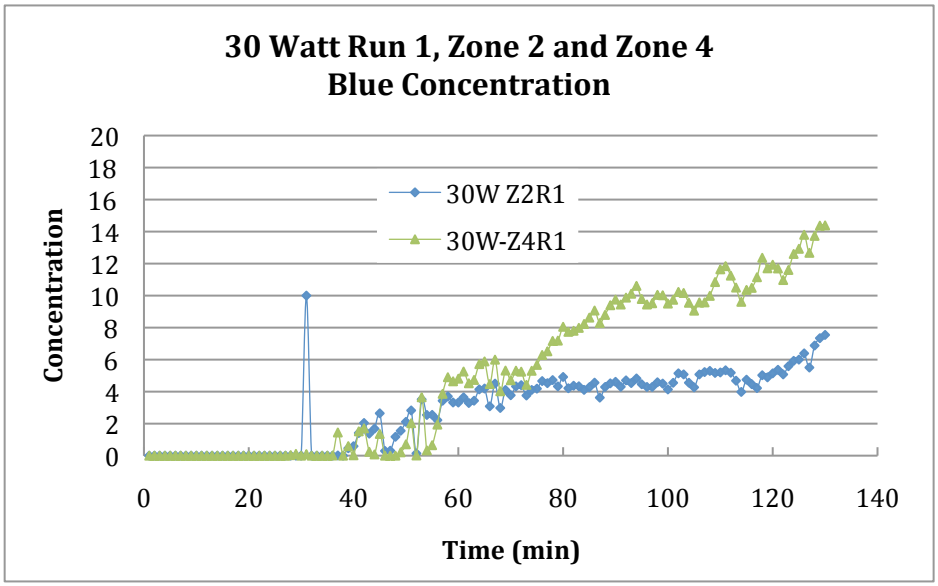

Figure 4.17: Zones 4 and 2, diverging concentrations in 10-Watt stimulated test, Spike indicates the start of stimulation

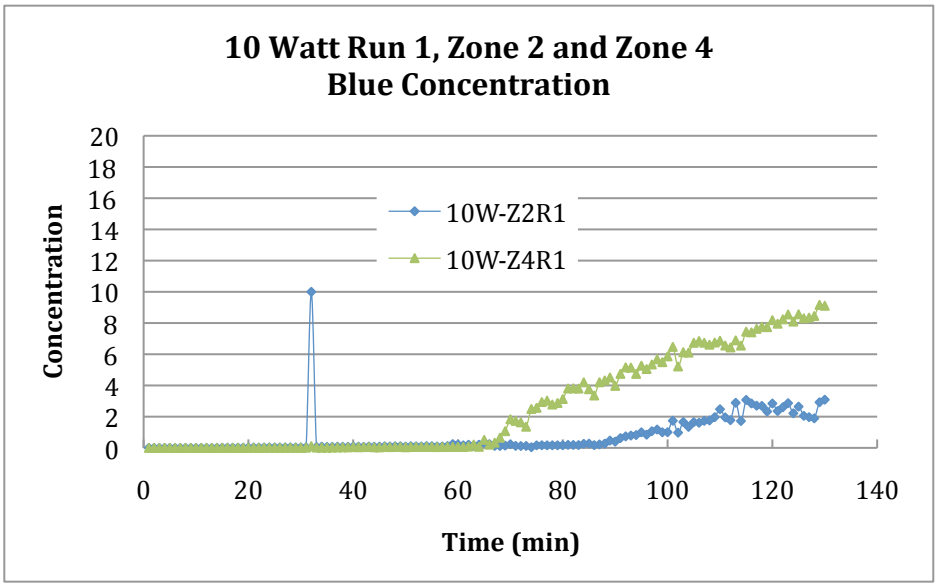

Figure 4.18: Zones 4 and 2, diverging concentrations in 10-Watt stimulated test, Spike indicates the start of stimulation

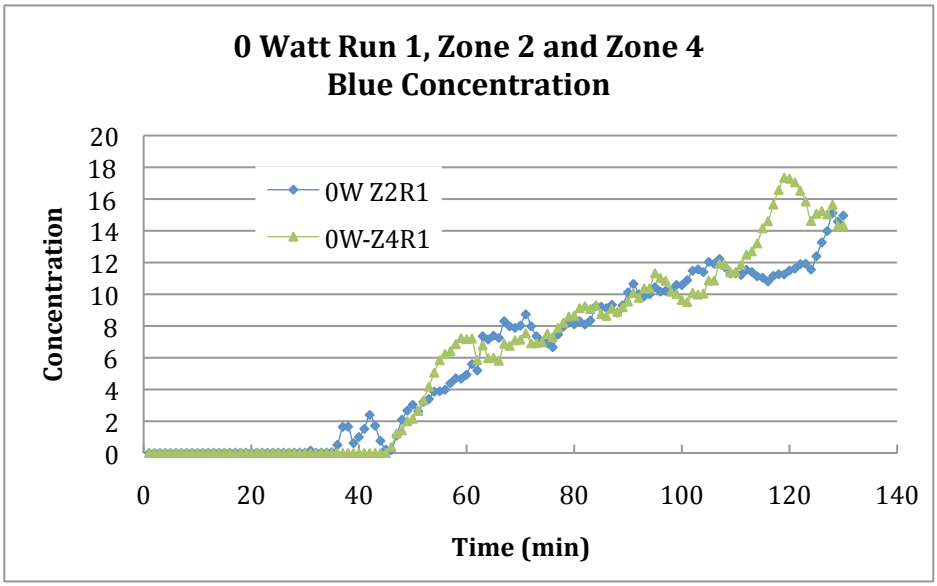

Figure 4.19: Zones 4 and 2, diverging concentrations in non-stimulated test

Other plots of red and blue concentration show similar patterns and can be seen in Appendix A. To further illustrate the difference because stimulated and non-stimulated conditions, the difference in concentration between Zones 4 and 2 are plotted. These plots

of red and blue shown in Figures 4.20 and 4.21 illustrate that with stimulation the concentrations diverge to the one side.

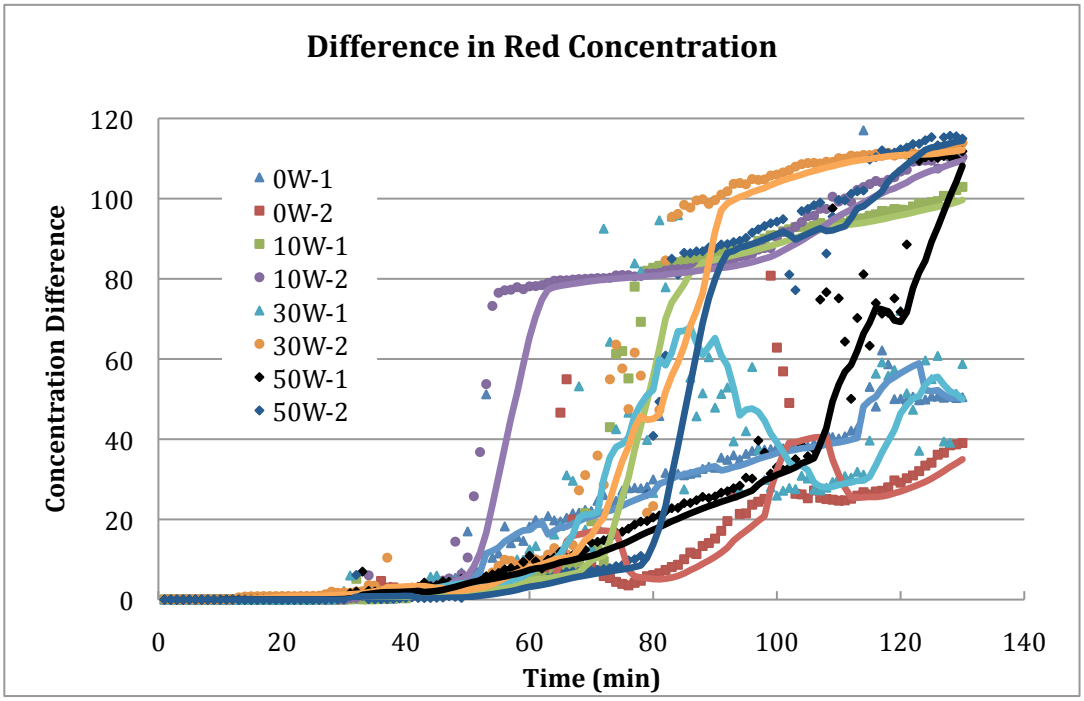

Figure 4.20: Red concentration difference between Zones 4 and 2, Average Trend Lines Added

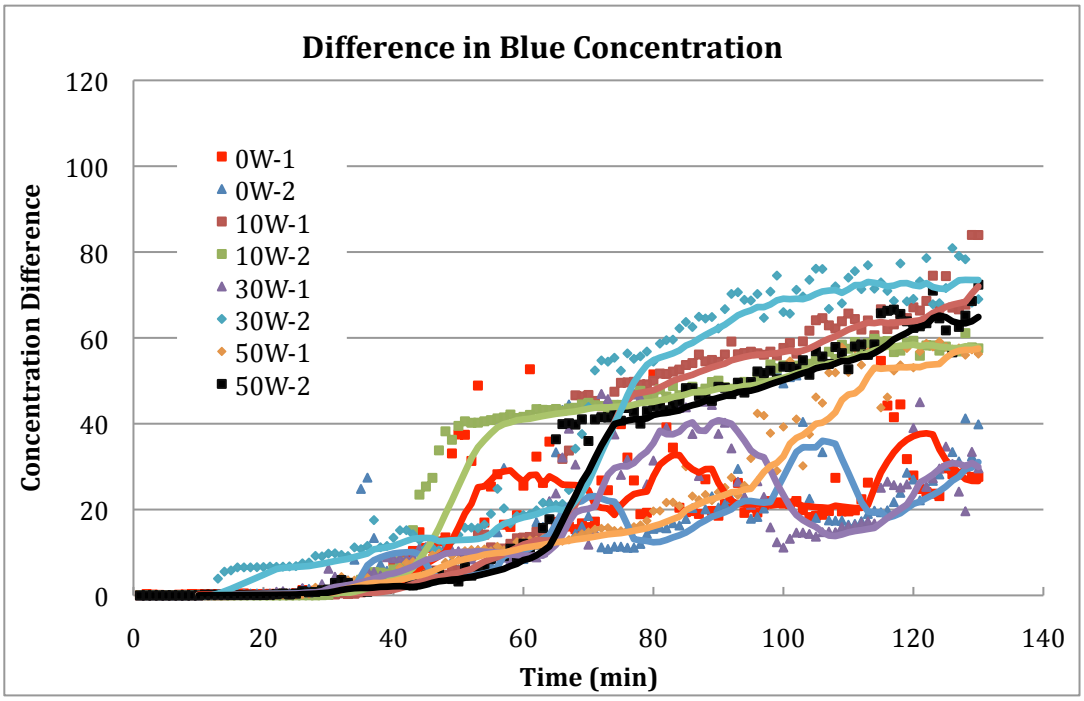

Figure 4.21: Blue concentration difference between Zones 4 and 2, Average Trend Lines Added

The effect of the stimulation is shown in Figure 4.20 and 4.21, where the concentration difference between Zones 2 and 4 is much greater in the stimulated test than the non-stimulated tests. This does show that there is an effect due to the stimulation on the dye concentration but further analysis of the dye concentration at each pixel, opposed to integrated in Zones 1 to 5 is needed to study where the effect is taking place and to see if there is a correlation to power, electric field, or their gradients.

The slope of the plot of concentration versus time is a representative of the rate of increase in concentration in a given zone and, therefore, is proportional to the rate of transport (transport flux) of the dye. Comparing the difference in transport flux rates between Zones 2 and 4 can be approximated by subtracting the slope of the best fit line of each plot. Using Microsoft Excel's linear trend line function, the slope of the concentration plot is found. The slope is only measured after the 60 minute mark to eliminate the artificial marking spike indicating the start of stimulation and the long flat portion of the curve associated with non-stimulation. An example of the trend lines used for analysis is shown in Figure 4.22.

The two above-mentioned slopes and their difference are compared but do not give a clear relationship to power. The differences in rate, measured as difference in slope, are shown in Figure 4.23, graphed versus RF power. The rates are consistent for each power but do not have a trend from which a relationship can be determined.

Looking at the individual concentration gradients in Zones 2 and 4 gives a better understanding of the cause of the difference between the two zones. In Figure 4.24, it can be seen that the rate of dye transport into Zone 4 is fairly consistent in all tests. This is

somewhat inconsistent with what is qualitatively seen in the images but could be explained by the contrast of the rate of dye transport into Zone 2, shown in Figure 4.25.

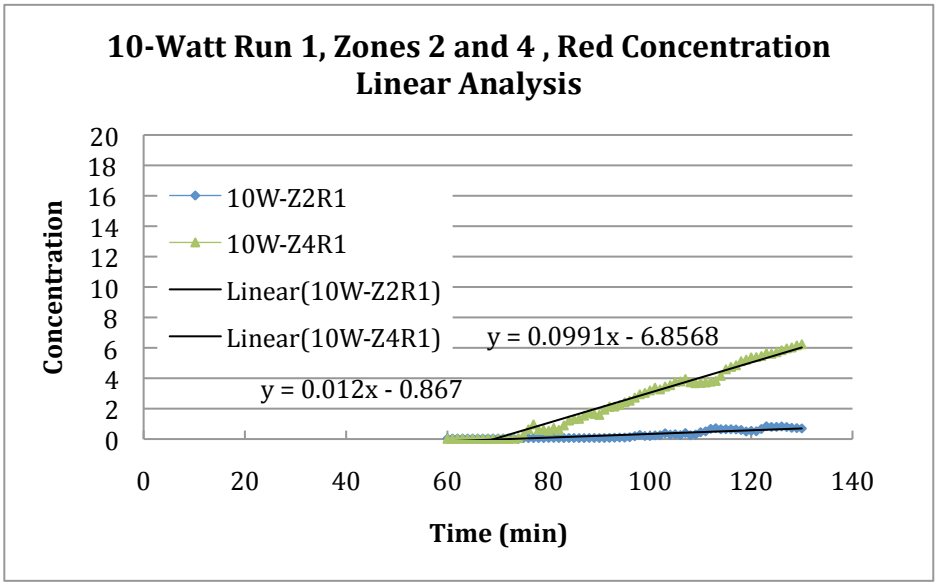

Figure 4.22: Linear fit-lines to concentration increases

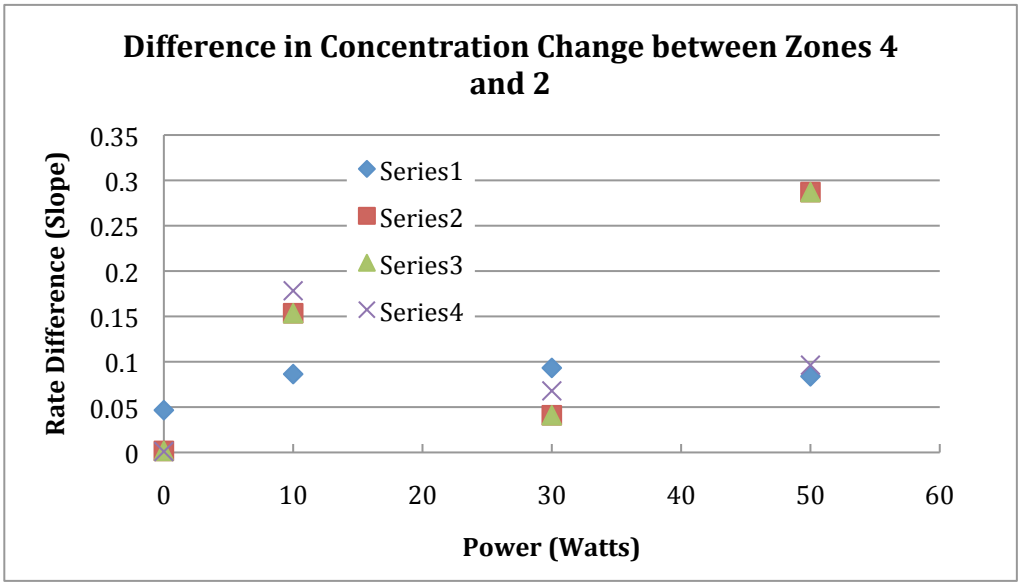

Figure 4.23: Concentration rate difference for all runs and all powers

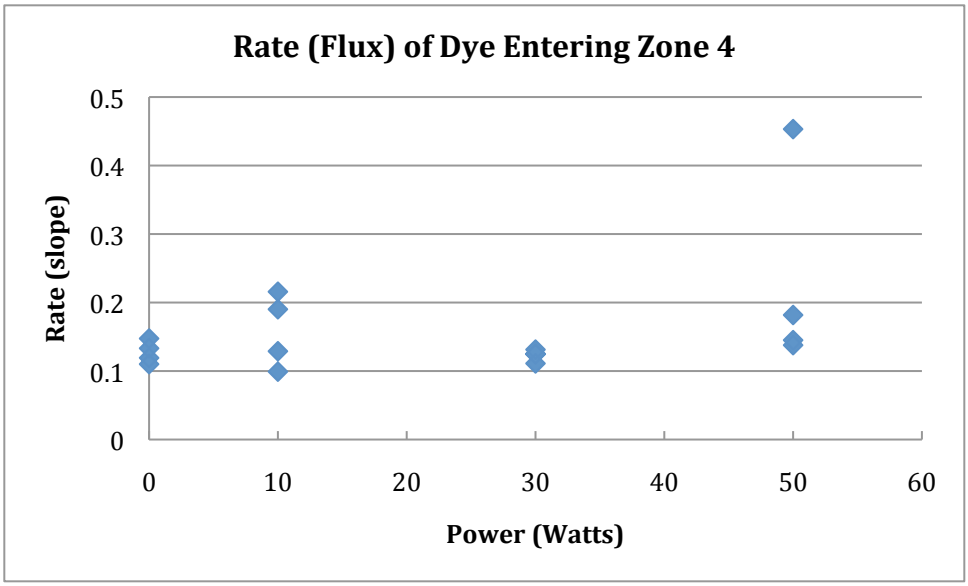

Figure 4.24: Rate (a representative of flux) of dye entering Zone 4 based on slopes of concentration plots

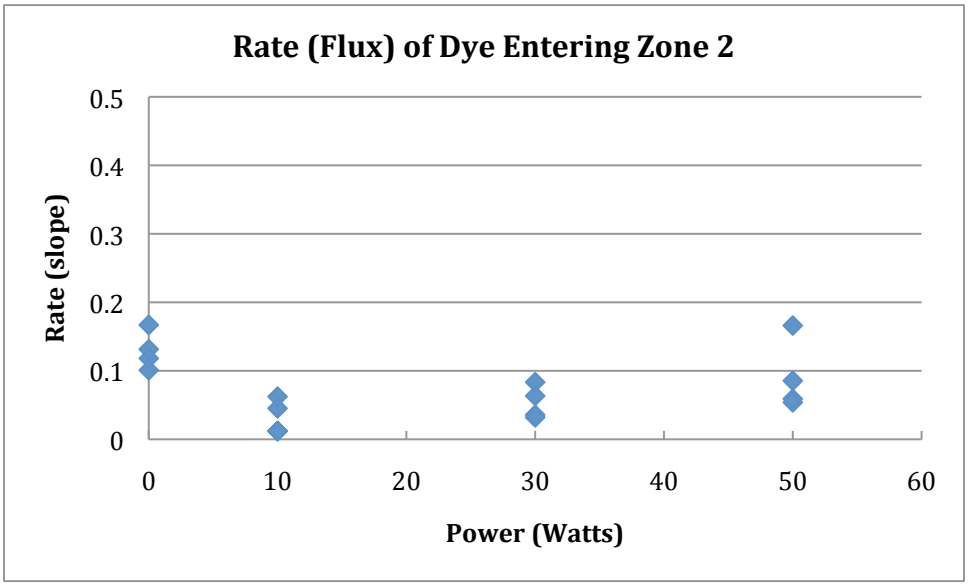

Figure 4.25: Rate (a representative of flux) of dye entering Zone 2 based on slopes of concentration plots

This analysis indicates that it is not the rate (flux) of dye entering Zone 4 that has changed but rather the rate (flux) of dye entering Zone 2 has been retarded by the stimulation.

5 CONCLUSIONS

This research is the initial stage in the first objective in the investigation of the effect of EM stimulation on air sparging. The data clearly shows that the use of EM stimulation does affect the movement of dye in the water. The ability to create a relationship between stimulation power (or electric field) and transport rates requires more analysis. This work is a good basis for continuing research into the mechanism creating the effects seen it this study. The experience gained and methods developed for this work can be modified and improved upon in the future studies.

There are years of continuing work that can be performed to analyze the effect of EM stimulation on water and its uses. The biggest improvement to the testing apparatus and procedure would be to employ a proper antenna design to create an easier method to theoretically model the EM-field and make computation and development of a correlation between the electric field and dye transport easier. Understanding and mapping the field will help to clarify the mechanisms occurring in the stimulated medium, but a proper antenna will show the full potential of this approach. There is not enough evidence to demonstrate that the governing flow mechanism is dielectrophoresis or dielectrophoresis mixed with any other flow mechanism (e.g., diffusion).

One positive relationship that can be useful for the air sparging applications is that with EM-stimulation more dye movement was shown and in a controlled manner proportional to the design of the antenna (source of electric field) radiation pattern.

If diffusion between air channels is a limiting factor in air sparging, being able to stimulate and move more contaminants to the MTZ or more air from the MTZ to the contaminated zone will expedite the remediation.

If it is assumed that dielectrophoresis is the driving force, then it can be assumed that the dye in this case has a higher dielectric permittivity than water, because it moved toward the area of high gradient. Negative dielectrophoresis is force that moving the particle to low gradient, which by definition of an antennas field would be toward lower field intensities. Comparing the field and the dye movement it is shown that to have dielectrophoresis be the controlling mechanism in these tests the particle would have to have a dielectric permittivity higher than water, which is at 81. Further investigation shows that majority of the dye is water followed by propylene glycol. Propylene Glycol has a dielectric permittivity of between 2 and 12 depending on the frequency, so the dielectric constant of the dye is less than water. If the dielectric constant is less that water, there should be negative dielectrophoresis and the dye should move to low field gradient. With our complex fields and actual concentrations unknown we cannot conclusively say whether dielectrophoresis or any other mechanism is the driving force in the dye transport. The information in this study should be used in further investigations to determine the controlling mechanism.

REFERENCES

Braida, W., and Ong, S. K. (2001). "Air sparging effectiveness: laboratory characterization of air-channel mass transfer zone for VOC volatilization," *Journal of Hazardous Materials,* B87, pp. 241-258.

Clayton, W. (1998). A field and laboratory investigation of air fingering during air sparging. *Ground Water Monitoring and Remediation* 18, no. 2 pp. 134-145.

Dupont, R. R. (1993). "Fundamentals of bioventing applied to fuel contaminated sites," *Environmental Progress,* Vol. 12, No. 1, pp. 45-53.

Elder, C., and Benson, C. H. (1999). *"*Air channel formation, size, and spacing, and tortuosity during air sparging," *Ground Water Monitoring & Remediation,* pp. 171-181.

Falta, R. W. (2001). *Steam flooding for environmental remediation*, Manuals and Reports on Engineering Practice, American Society of Civil Engineers (0734-7685), (100), 153 p.

Fick, A. (1855), *On liquid diffusion*, Philosophical Magazine and Journal of Science, (10), 31-39

Fourier, Joseph. (1822). *Theorie Analytique de la Chaleur*. Firmin Didot (reissued by Cambridge University Press, 2009; ISBN 978-1-108-00180-9)

Jamieson, K. S., ApSimon, H. M., and Bell, J. N. B. (2007). "Electrostatics in the environment: how they may affect health and productivity," *Journal of Physics: Conference Series*, pp. 1-7.

Price, S. L., Kasevich, R. S., Johnson, M. A., Wilberg, D., and Marley, M. C. (1999). "Radio Frequency heating for Soil Remediation," *Journal of the Air and Waste Management Association*, Vol. 49, pp. 136-145.

Rutherford, K., and Johnson, P. (1996). "Effect of process control changes on aquifer oxygenation rates during in situ air sparging in homogeneous aquifers." *Ground Water Monitoring and Remediation,* Vol. 16, No. 2, pp. 131-138.

Semer, R., Adams, J. A., and Reddy, K. R. (1998). "An experimental investigation of airflow patterns in saturated soils during air sparging," *Geotechnical and Geological Engineering,* Vol. 16, pp. 59-75.

Tsai,Y. (2007) "Airflow paths and porosity/permeability change in a saturated zone during in situ air sparging" *Journal of Hazardous Materials,"* Vol. 142, pp. 315-323.

Vaid, Y. P., and Negussey, D. (1998). "Preparation of reconstituted sand specimens," *Advanced triaxial testing of soil and rock, ASTM STP 977*, Philadelphia, pp. 405-417.

Vermeulen, F., and McGee, B. (2000). "In Situ Electromagnetic Heating for Hydrocarbon Recovery and Environmental Remediation," *Journal of Canadian Petroleum Technology,* Vol. 39, No. 8, pp. 25-29.

Weingardt, K., and Gonzales, M. (2002). "Soil and Groundwater Remediation at an Abandoned Fuel Farm (Site 7) using Vacuum-Enhanced Pumping, Naval Air Facility, El Centro, California," *Soil and Sediment Contamination: An International Journal*, Vol. 11. No. 3, pp. 390-391.

APPENDIX A

Dye Movement Sample

50-Watt EM-Stimulation 5-min intervals

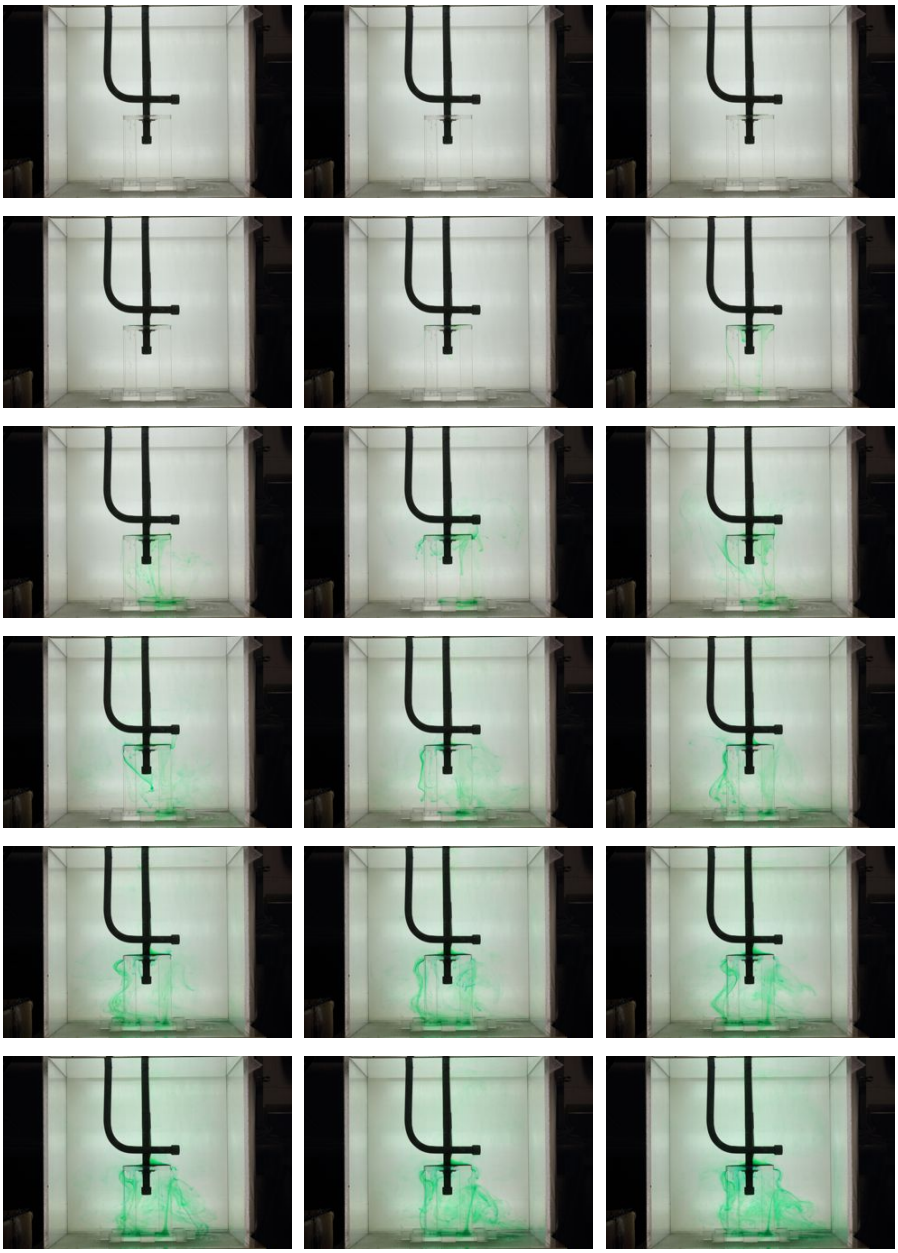

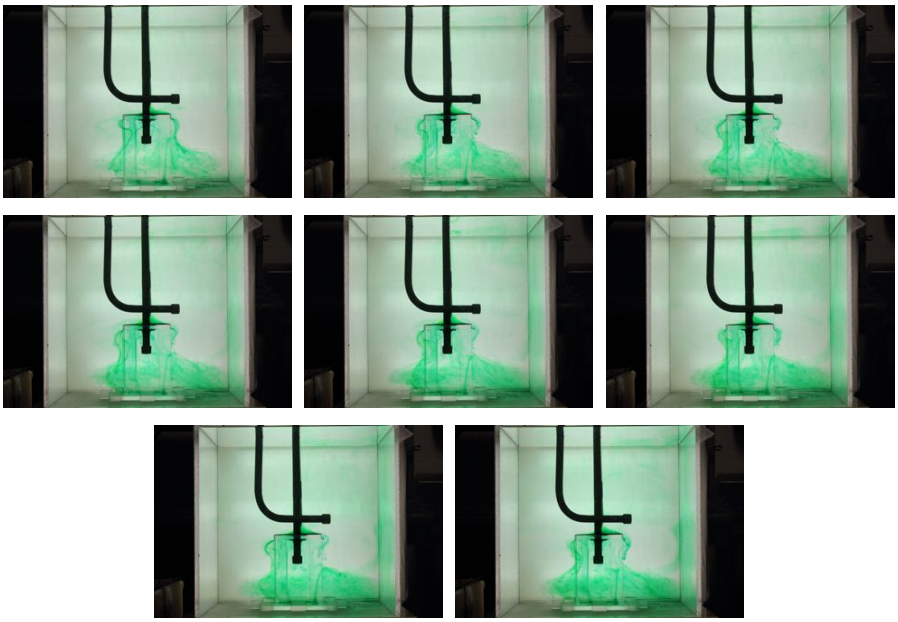

No EM-Stimulation 5-min intervals